nature cell biology

A cell-intrinsic role for TLR2–MYD88 in intestinal and breast epithelia and oncogenesis

Ferenc A. Scheeren[1,2,8], Angera H. Kuo[1,8], Linda J. van Weele[1], Shang Cai[1], Iris Glykofridis[2], Shaheen S. Sikandar[1], Maider Zabala[1], Dalong Qian[1], Jessica S. Lam[1], Darius Johnston[1], Jens P. Volkmer[1], Debashis Sahoo[1,9], Matt van de Rijn[3], Frederick M. Dirbas[4], George Somlo[5], Tomer Kalisky[6,9], Michael E. Rothenberg[1], Stephen R. Quake[6] and Michael F. Clarke[1,7,10]

It has been postulated that there is a link between inflammation and cancer. Here we describe a role for cell-intrinsic toll-like receptor-2 (TLR2; which is involved in inflammatory response) signalling in normal intestinal and mammary epithelial cells and oncogenesis. The downstream effectors of TLR2 are expressed by normal intestinal and mammary epithelia, including the stem/progenitor cells. Deletion of MYD88 or TLR2 in the intestinal epithelium markedly reduces DSS-induced colitis regeneration and spontaneous tumour development in mice. Limiting dilution transplantations of breast epithelial cells devoid of TLR2 or MYD88 revealed a significant decrease in mammary repopulating unit frequency compared with the control. Inhibition of TLR2, its co-receptor CD14, or its downstream targets MYD88 and IRAK1 inhibits growth of human breast cancers *in vitro* and *in vivo*. These results suggest that inhibitors of the TLR2 pathway merit investigation as possible therapeutic and chemoprevention agents.

Microbial pathogens trigger inflammatory response through pattern-recognition receptors, resulting in the activation of the innate immune system[1–5]. Toll-like receptors (TLRs) are among the best characterized pattern-recognition receptors. In addition to microbial ligands, a number of endogenous ligands, including intracellular components released after apoptosis and cell death, can stimulate TLRs. This suggests a role for TLRs other than directly recognizing and responding to microbes[2,4,5]. CD14 is a GPI-linked protein that is found on the surface of many TLR4- and/or TLR2-expressing cells[6–9]. Once ligands bind to CD14, signal transduction takes place through TLR2 and TLR4.

Inflammatory response can play a role in cancer (for example, TLR2-induced inflammatory response in myeloid cells can affect tumour progression and metastasis)[2–6,10–14]. Moreover, myeloid differentiation primary response protein-88 (MYD88), an adaptor protein for TLRs and IL-1R in innate immune cells[15], is crucial for spontaneous intestinal tumour formation[14] and has activating oncogenic mutations in diffuse large B cell lymphoma and chronic lymphocytic leukaemia[16,17]. Other examples linking inflammation and cancer are: chronic gastritis due to *Helicobacter pylori* infection is a major risk for gastric cancer and chronic colitis often leads to colorectal cancer[18–21].

Transplantation and lineage-tracing data suggested the presence of multi-potent mammary stem cells (MSCs) and progenitors and showed that a single MSC is able to reconstitute a functional mammary gland[22–30]. MSCs reside at the top of the mammary cellular proliferation hierarchy; however, molecular pathways regulating their self-renewal are not well characterized.

The intestinal epithelium consists of long-lived stem cells (resides near the crypt bottom) with self-renewal capacity. Two types of stem cell are proposed in small intestinal crypts: cycling crypt base columnar cells and quiescent +4 cells. As in the breast, regulators of stem cell self-renewal in intestinal epithelium are poorly understood[2,3,6,8,10–15,19,21,31–39]. We show that TLR2/CD14 signalling through MYD88 is an important pathway for regeneration of intestinal epithelial cells after inflammation damage, regeneration of mammary epithelium, and growth of some cancers. Our data reveal that inhibitors of the TLR pathway warrant therapeutic exploration in the treatment or chemoprevention of breast and colon cancer.

[1]Stanford Institute for Stem Cell Biology and Regenerative Medicine, Stanford University, 265 Campus Drive, Stanford, California 94305, USA. [2]The Netherlands Cancer Institute, 1066 CX Amsterdam, The Netherlands. [3]Department of Pathology, Stanford University, Stanford, California 94305, USA. [4]Department of Surgery, Stanford University, Stanford, California 94305, USA. [5]Department of Medical Oncology, Beckman Research Institute and City of Hope Comprehensive Cancer Center, Duarte, California 91010, USA. [6]Department of Bioengineering and Howard Hughes Medical Institute, Stanford University, Stanford, California 94305, USA. [7]Department of medicine, Division of Oncology, Stanford University, Stanford, California 94305, USA. [8]These authors contributed equally to this work. [9]Present addresses: Department of Pediatrics, University of California at San Diego, La Jolla, California 92093, USA (D.S.); Faculty of Engineering, Bar-Ilan University, Ramat Gan 52900, Israel (T.K.)
[10]Correspondence should be addressed to M.F.C. (e-mail: mfclarke@stanford.edu)

Received 31 July 2014; accepted 29 September 2014; published online 2 November 2014; DOI: 10.1038/ncb3058

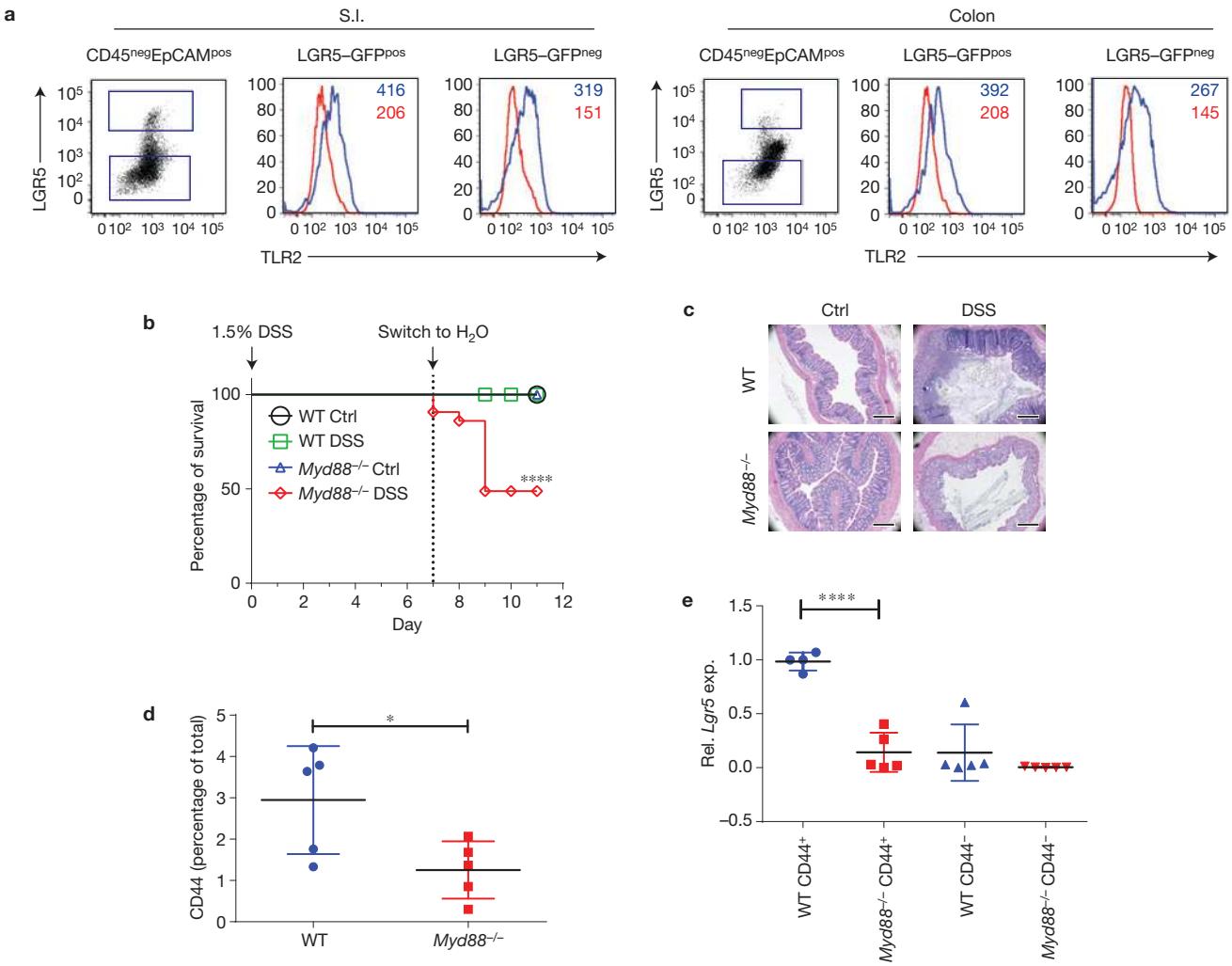

Figure 1 TLR2 and MYD88 are functional in murine intestinal epithelial cells. (**a**) Representative flow cytometry histogram of TLR2 on small intestine (S.I.) and colon (DAPI^{neg} CD45^{neg} EpCAM^{pos}) Lgr5–GFP^{pos} cells; red is the isotype control for each specific sub-population, and blue is the TLR2 staining. Median fluorescence is shown for each histogram. Data are representative of 4 mice. (**b**) WT and *Myd88*$^{-/-}$ mice were given normal drinking water or 1.5% DSS in drinking water for 7 days (WT Ctrl: $N=9$ mice; WT DSS: $N=28$, *Myd88*$^{-/-}$ Ctrl: $N=8$; *Myd88*$^{-/-}$ DSS: $N=43$). Mice were changed to normal drinking water on day 8. Survival was monitored for 11 days. These data are combined from 3 different experiments. $^{****}P<0.0001$. (**c**) Representative photo of H&E staining of colons from WT and *Myd88*$^{-/-}$ mice at day 11 (scale bars, 0.5 mm). Data are representative of 8 mice. (**d**) Percentage of CD44 on colonic cells as determined by flow cytometry between DSS-treated WT ($N=4$) and *Myd88*$^{-/-}$ ($N=5$) mice. $^{*}P=0.0337$. (**e**) qPCR for *Lgr5* expression on epithelial CD44^{pos} and CD44^{neg} sorted populations of WT ($N=4$) and *Myd88*$^{-/-}$ ($N=5$) mice. $^{****}P<0.0001$. Values represent mean ± s.d. Student's unpaired *t*-test for independent samples was used.

RESULTS

Epithelial-specific TLR2–MYD88 signalling in the intestinal tract

We first examine the role of TLR2 signalling in the intestine because this pathway has been linked to homeostasis of intestinal epithelial cells[39,40]. Flow cytometry analysis of intestinal cells isolated from Lgr5–GFP mice demonstrated that Lgr5–GFP^{pos}EpCAM^{pos}CD45^{neg} cells, which are enriched for intestinal stem cells, expressed slightly higher levels of TLR2 as compared with Lgr5–GFP^{neg}EpCAM^{pos}CD45^{neg} cells (Fig. 1a). This shows that TLR2 is expressed by the LGR5^{pos} intestinal stem cells.

The epithelium of the intestines is constantly self-renewing and will quickly regenerate after injury. To study the regenerative capacity of TLR2 signalling in colonic epithelium, we subjected *Myd88*$^{-/-}$ mice to dextran sodium sulphate (DSS) to induce acute colitis. In this model, administration of DSS in drinking water may result in weight loss, bloody diarrhoea and eventual death. These clinical manifestations are the results of epithelial barrier dysfunction, degeneration and necrosis with consequent recruitment and activation of inflammatory cells in the colon[41–43]. Withdrawal of DSS in drinking water induces the regeneration of the colon that includes rapid crypt hyperplasia and fission. *Myd88*$^{-/-}$ and wild-type (WT) mice were treated with 1.5% DSS for 7 days (Day 0 to Day 7) to induce acute colitis and then switched back to normal drinking water to promote regeneration (Day 8 to Day 11). Consistent with published data[40,44], *Myd88*$^{-/-}$ mice are more susceptible to DSS-induced colitis as exhibited by higher morbidity as compared with WT (Fig. 1b). Furthermore, DSS-treated mice from the regeneration period (Day 11) revealed that

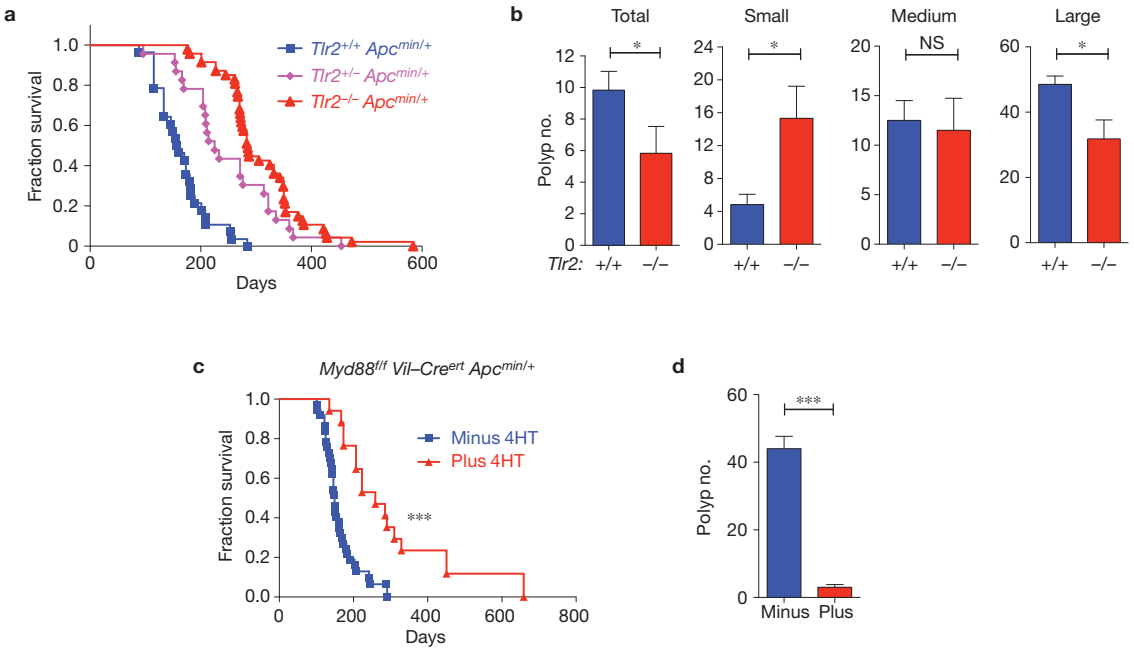

Figure 2 TLR2 and MYD88 protect $Apc^{min/+}$ mice from adenomas. (**a**) Kaplan–Meier survival curve showing $Tlr2^{+/+}Apc^{min/+}$ ($N=28$ mice), $Tlr2^{+/-}Apc^{min/+}$ ($N=23$) $P<0.001$ and $Tlr2^{-/-}Apc^{min/+}$ ($N=47$) $P<0.001$. Median survival rates of $Tlr2^{+/+}Apc^{min/+}$, $Tlr2^{+/-}Apc^{min/+}$ and $Tlr2^{-/-}Apc^{min/+}$ mice are 157, 225 and 285 days, respectively. (**b**) Total number of visible polyps ($^{*}P=0.024$) and number of small ($^{*}P=0.028$), medium (NS, not significant) and large polyps ($^{*}P=0.05$) in the S.I. and colon was quantified in age (16–20 weeks old)-matched $Tlr2^{+/+}Apc^{min/+}$ (blue; $N=12$) and $Tlr2^{-/-}Apc^{min/+}$ (red; $N=6$) mice. Analysis of the visible polyps in the intestinal tract showed that *Tlr2* deficiency resulted in a significantly decreased tumour burden with decreased large polyps and increased smaller-sized polyps as compared with wild-type. (**c**) Kaplan–Meier survival curve showing $Myd88^{f/f}$ *Vil–*Cre^{ert2} $Apc^{min/+}$ mice not treated with 4HT (blue, $N=35$) and mice treated with 4HT (red, $N=15$), $P<0.001$. (**d**) Total number of visible polyps in S.I. and colon was quantified at 12 weeks after 4HT injection, $^{***}P<0.001$ ($N=4$ mice). Values represent mean ± s.d. Student's unpaired *t*-test for independent samples was used.

$Myd88^{-/-}$ had more severe crypt loss and deterioration of crypt–villus architecture, and less crypt hyperplasia and fission (Fig. 1c). Flow cytometry analysis of the colon epithelial cells ($EpCAM^{pos}$) from DSS-treated mice revealed a decrease in expression of CD44, which labels the intestinal crypt base that contains stem cells and progenitors, in $Myd88^{-/-}$ versus WT mice (Fig. 1d). Expression of Lgr5, which marks the proliferative intestinal stem cell, has been shown to be important for intestinal regeneration after injury[1,45–47]. To ascertain whether the expression of *Lrg5* is affected, we performed *Lgr5* qPCR on flow-sorted $EpCAM^{pos}CD44^{pos}$ cells from DSS-treated mice on Day 9. The expression of *Lgr5* is significantly reduced in DSS-treated $Myd88^{-/-}$ versus WT mice (Fig. 1e). These data suggest that the TLR–MYD88 pathway may play a role in the expansion of the intestinal $LGR5^{pos}$ stem cell pool critical for after injury.

TLR2–MYD88 protects $Apc^{min/+}$ mice from adenomas

$LGR5^{pos}$ intestinal stem cells are reported to be the cells of origin of adenoma initiated by adenomatous polyposis coli (*Apc*) mutations[48–53]. Moreover, it has been shown that ablation of MYD88 protects $Apc^{min/+}$ mice from developing intestinal tract tumours[14,54–56]. Confirming that TLR2 is involved in the protection conferred by MYD88, $Tlr2^{-/-}Apc^{min/+}$ mice have reduced mortality and polyp formation compared with $Apc^{min/+}$ littermates (Fig. 2a,b). Deletion of *Tlr2–Myd88* in the mouse could protect mice from adenoma formation indirectly through the innate immune system, directly through effects on epithelial cells, or both.

To assess whether there is an intestinal epithelial-specific component, we investigated whether deletion of MYD88 in epithelial cells, which should dampen all TLR signalling, can also protect $Apc^{min/+}$ mice from adenoma formation. We developed $Myd88^{f/f}$ *Vil–*CRE^{ert2} $Apc^{min/+}$ mice, and induced Cre^{ert2} with tamoxifen at the weaning age. Consistent with reports on the mortality of $Apc^{min/+}$ mice, un-induced $Myd88^{f/f}$ *Vil–*Cre^{ert2} $Apc^{min/+}$ mice developed intestinal tumours and died within the age of 5–6 months. When MYD88 was ablated in a *Vil–*Cre^{ert2}-specific manner, median survival of $Apc^{min/+}$ mice went from 149 to 259 days (Fig. 2c). After 16 weeks of tamoxifen induction, the number of polyps was extensively reduced when MYD88 was ablated as compared with the control (Fig. 2d). These data suggest that the TLR-signalling component MYD88, at least partly, affects the epithelial stem cells and contributes in a cell-intrinsic manner to the mortality and morbidity caused by inactivation of *Apc* in intestinal tumours.

TLR2–CD14–MYD88 complex in the mammary epithelium

We postulated that other epithelia, such as the breast epithelium, might also contain a stem cell compartment that uses the TLR pathway. We began by addressing whether TLR2 was expressed on murine mammary epithelial cells (MECs). Using published markers of murine MECs (mammary repopulating units (MRUs: $CD24^{pos}$, $CD49f^{pos}$), myo-epithelial cells (MYOs: $CD24^{dim}CD49f^{pos}$), luminal progenitor cells (Ma-CFCs: $CD24^{pos}CD49f^{neg}CD61^{pos}$) and mature luminal cells (EPIs: $CD24^{pos}$, $CD49f^{min}$, $CD61^{neg}$); refs 24,25,57–59), we found that

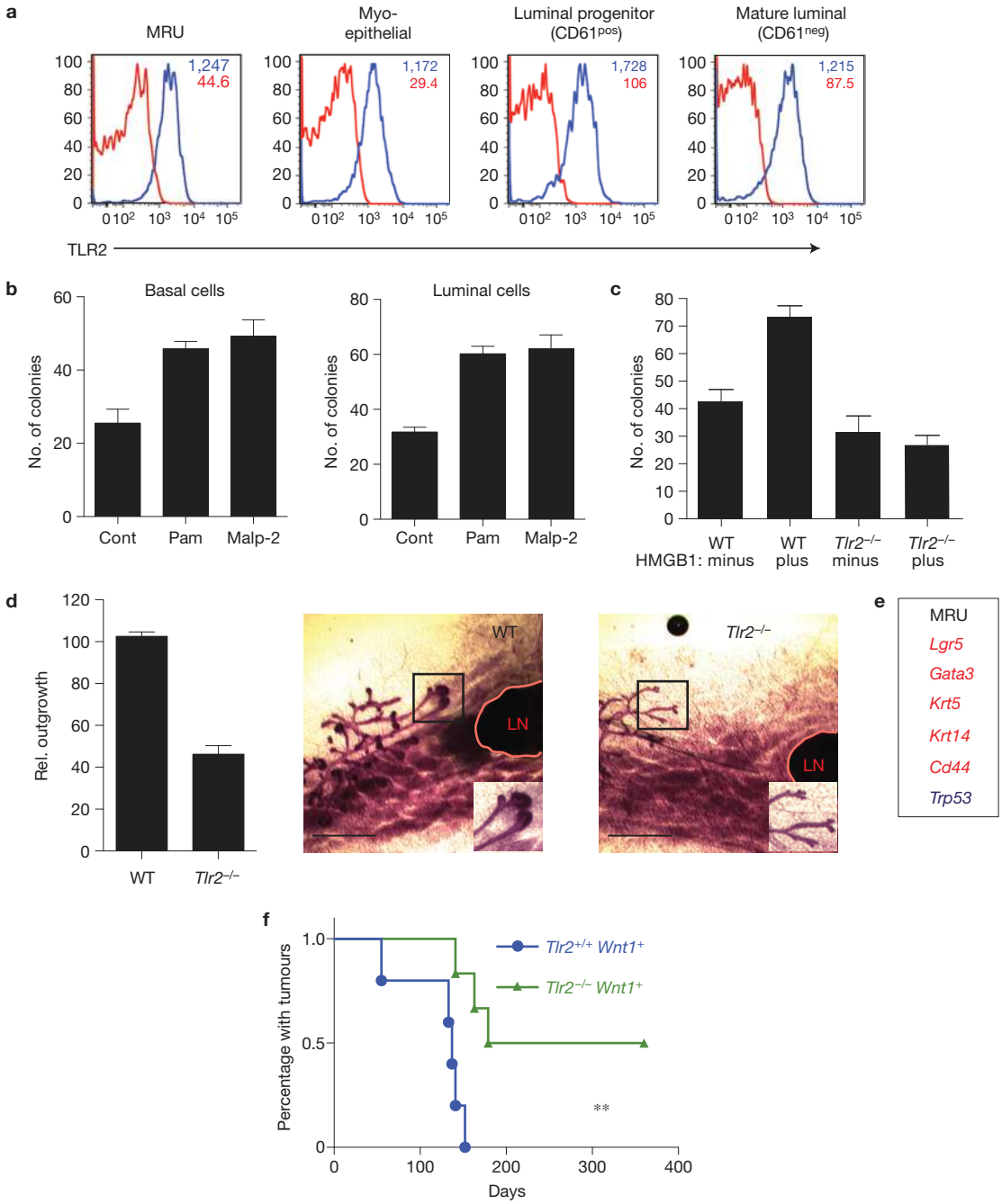

Figure 3 TLR2 is functionally expressed in normal murine mammary epithelial cells. (**a**) Representative flow cytometry histogram showing staining for TLR2 (red) and the isotype control (blue) for each specific sub-population. Median fluorescence is shown for each histogram. Data are representative of 4 mice. (**b**) Matrigel *in vitro* colony-forming capacity of luminal and basal cells with Pam3CSK4 and Malp-2. Basal cells: Cont (control) versus Pam: $P=0.0035$; Cont versus Malp-2; $P=0.007$. Luminal cells: Cont versus Pam: $P=0.0001$; Cont versus Malp-2: $P=0.001$. (**c**) Sorted Ma-CFCs from WT mice and *Tlr2*$^{-/-}$ mice in a 2D colony-forming assay with or without HMGB1. WT control versus WT HMGB1: $P=0.0001$. Experiments in **b**,**c** were repeated twice with $N=4$ mice in total. (**d**) Carmine Alum-stained inguinal mammary glands of 22-day-old mice, WT and *Tlr2*$^{-/-}$ mice. Lymph node (LN). Representative photograph is shown; data are representative of 8 mice. Scale bar, 1 mm. (**e**) List of differentially expressed genes based on single-cell PCR of MRUs ($N=2$). (**f**) Kaplan–Meier survival curve showing *Tlr2*$^{+/+}$*Wnt1*$^{+}$ ($N=6$ mice) and *Tlr2*$^{-/-}$*Wnt1*$^{+}$ ($N=6$ mice) $^{**}P<0.03$. Values represent mean ± s.d. Student's unpaired *t*-test for independent samples was used.

TLR2 was expressed in all populations (Fig. 3a). We next confirmed expression of TLR2 and its downstream adaptor MYD88 by qPCR on flow-sorted populations. Increased *Tlr2* expression was found in the Ma-CFC, MRU and MYO populations versus the mature luminal population. *Myd88* expression was similar in all populations (Supplementary Fig. 1a,b).

To investigate whether TLR2 has a functional role in MECs, we examined the effect of known TLR2 ligands (Pam3CSK4

activates TLR2/1; Malp-2 activates TLR2/6) in an *in vitro* colony-forming assay. Basal cells ($CD24^{dim/pos}CD49f^{pos}$) and luminal cells ($CD24^{pos}CD49f^{neg/dim}$) were sorted and plated on Matrigel with or without TLR2 stimulation (Fig. 3b). Each ligand increased colony formation of both luminal and basal cells. More importantly, HMGB1, an endogenous TLR2 ligand that is released on cell death, increased colony formation of flow-sorted Ma-CFCs from a WT mouse but not from a $Tlr2^{-/-}$ mouse (Fig. 3c). Without HMGB1, WT and $Tlr2^{-/-}$ Ma-CFCs had similar levels of colony formation (Fig. 3c and Supplementary Fig. 1c). Next, we determined whether TLR2 has a functional role *in vivo* by analysing ductal outgrowth in mammary glands of 4–6-week-old $Tlr2^{-/-}$ mice, which corresponds to puberty. WT mice showed a ductal tree with terminal end buds almost reaching the lymph nodes at day 22 post-partum. In contrast, the development of the age-matched ductal tree in the $Tlr2^{-/-}$ mice was severely inhibited (Fig. 3d) and only a few terminal end buds were observed. $Tlr2^{-/-}$ epithelial ducts showed decreased invasion of the fat pad at day 22 post-partum but not at week 6–8. In addition, flow cytometry analysis and immunohistochemistry of 6-week-old mammary glands and mammary whole-mounts of lactating WT and $Tlr2^{-/-}$ mice showed no appreciable difference (Supplementary Fig. 2a–c).

As for intestine, deletion of *Tlr2* could affect MECs by a cell-extrinsic manner, cell-intrinsic manner, or both. To determine whether the MRU compartment was affected by the absence of TLR2 in a cell-intrinsic manner, we performed transplantation experiments. We transplanted sorted lineage-negative (lin^{neg}) cells from WT or $Tlr2^{-/-}$ mice into recipient WT mice and found that $Tlr2^{-/-}$ mice have decreased frequency of MRUs as determined by the outgrowth of the mammary epithelial tree (Fig. 4a and Supplementary Fig. 3a). Furthermore, limiting dilution transplantation of sorted MRUs of $Tlr2^{-/-}$ and secondary transplants of outgrowths from the MRU transplants also exhibited decreased outgrowth of the mammary epithelial tree as compared with WT (Fig. 4b–d). The outgrowth defects occurred in mice whose immune systems are WT suggesting that there is a decreased number of MRUs in $Tlr2^{-/-}$ mice and TLR signalling has a cell-intrinsic component that is not solely due to signalling defects of innate immune cells.

The role of the TLR2 co-activator CD14 in MECs was investigated next[7,9]. The expression of CD14 in different populations of murine MECs was measured (Supplementary Fig. 2d). Consistent with published results we find that luminal cells consist of a $CD14^{pos}$ and a $CD14^{neg}$ population[23]. Luminal $CD14^{pos}$ cells have been described to be progenitors as this population has the capacity to form colonies *in vitro*. Intriguingly, MYOs as well as MRUs also expressed CD14, although at a lower level. As for WT and $Tlr2^{-/-}$ mice, flow cytometry analysis and immunohistochemistry of 6-week-old mammary glands and mammary whole-mounts of lactating $Cd14^{-/-}$ mice showed no appreciable difference (Supplementary Fig. 2a–c). Limiting dilutions of sorted lin^{neg} and MRUs revealed that there is a reduction in MRU frequency when *Cd14* is ablated in the MECs (Fig. 4a–c and Supplementary Fig. 3a). TLR4 was also expressed in all 4 populations (Supplementary Fig. 2d). Our transplant studies of $Tlr4^{-/-}$ mice revealed a decreased MRU frequency (Supplementary Fig. 3b,c), although not as significant as that observed for $Tlr2^{-/-}$ and $Cd14^{-/-}$ mice. Together these data suggest that TLR2, CD14 and TLR4 are functionally expressed on murine MECs and that they affect the MRU function.

To confirm that MYD88 has a function in the MRU compartment independent of signalling from innate immune cells, we analysed $Myd88^{-/-}$ MECs of cytokeratin-14 ($K14$–$Cre^{pos}Myd88^{f/f}$ mice. Analysis of the *K14–Cre* mouse revealed that both luminal and myoepithelial cells arise from $K14^{pos}$-expressing progenitors[28]. Limiting dilution transplantation of sorted lin^{neg} cells from $K14$–$Cre^{pos}Myd88^{f/f}$ and $K14$–$Cre^{neg}Myd88^{f/f}$ mice revealed a 24-fold reduction in the MRU frequency when MYD88 is ablated in MECs (Fig. 4e,f). These data suggest that MYD88 could play a role in the function of mammary stem cells. Immunohistochemistry of the *Myd88*-deficient mammary glands demonstrated that the mammary gland remains intact (Supplementary Fig. 2e,f).

IL-1R1 and IL-18R are also upstream of MYD88 (ref. 15); hence, we examine whether they have a role in the decreased transplant efficiency of $Tlr2^{-/-}$ and $Cd14^{-/-}$ cells. Flow cytometry analysis showed that IL-1R1 is expressed on MRUs and Ma-CFCs whereas IL-18R is expressed only on the Ma-CFCs. (Supplementary Fig. 2d). Limiting dilution transplantation of sorted lin^{neg} cells from $Il\text{-}1r1^{-/-}$ and $Il\text{-}18r^{-/-}$ mice did not show a decreased MRU frequency (Supplementary Fig. 3d). These results suggest that although MYD88 is a downstream effector of TLR2, CD14, IL-1R1 and IL-18R signalling, the signal for efficient function of MRU is through the TLR2/CD14 pathway.

Single-cell analysis of MECs

Owing to a significant reduction of MRUs in $Tlr2^{-/-}$ MECs, we reasoned that these cells may express altered levels of genes involved in self-renewal. We examined the expression of a number genes involved in self-renewal in WT and $Tlr2^{-/-}$ cells using single-cell qPCR. MRUs, MYOs, Ma-CFCs and EPIs were double sorted for single-cell qPCR. Hierarchical clustering was performed according to the similarity of their gene expression. Although similar clusters were observed a number of genes that are involved in self-renewal were differentially expressed in the MRUs between WT and $Tlr2^{-/-}$ mice (Fig. 3e and Supplementary Fig. 4). The upregulation of *Trp53* prompted us to investigate whether the *Ink4a/Arf* locus is functionally involved in the reduction of MRU in the $Tlr2^{-/-}$ mice. As previously published, *Ink4a/Arf* deficiency did not affect the MRU frequency, suggesting that INK4A/ARF levels in WT stem and progenitor cells are negligible[18]. Importantly, *Ink4a/Arf* deficiency resulted in a rescue of MRU frequency of the $Tlr2^{-/-}$ cells (Supplementary Figs 3e,f). These data suggest that MRUs are affected by TLR2.

TLR2 in development of mammary tumours

To determine whether TLR2 affects *in vivo* breast cancer development, MMTV–Wnt1 transgenic mice were bred on a $Tlr2^{-/-}$ background. $Tlr2^{-/-}$MMTV–Wnt1 ($Tlr2^{-/-}Wnt1$) mice have a markedly reduced tumour formation compared with $Tlr2^{+/+}$MMTV–Wnt1 ($Tlr2^{+/+}Wnt1$) littermates (Fig. 3f). Median tumour-free days of $Tlr2^{+/+}Wnt1$ and $Tlr2^{-/-}Wnt1$ are 137 and 269 days respectively. These data suggest that TLR2 is involved in *de novo* mammary tumour formation.

TLR signalling in human breast and colon cancer

Given the possible role of TLRs in normal murine colon and breast epithelial stem cells, and in murine intestinal and breast tumours,

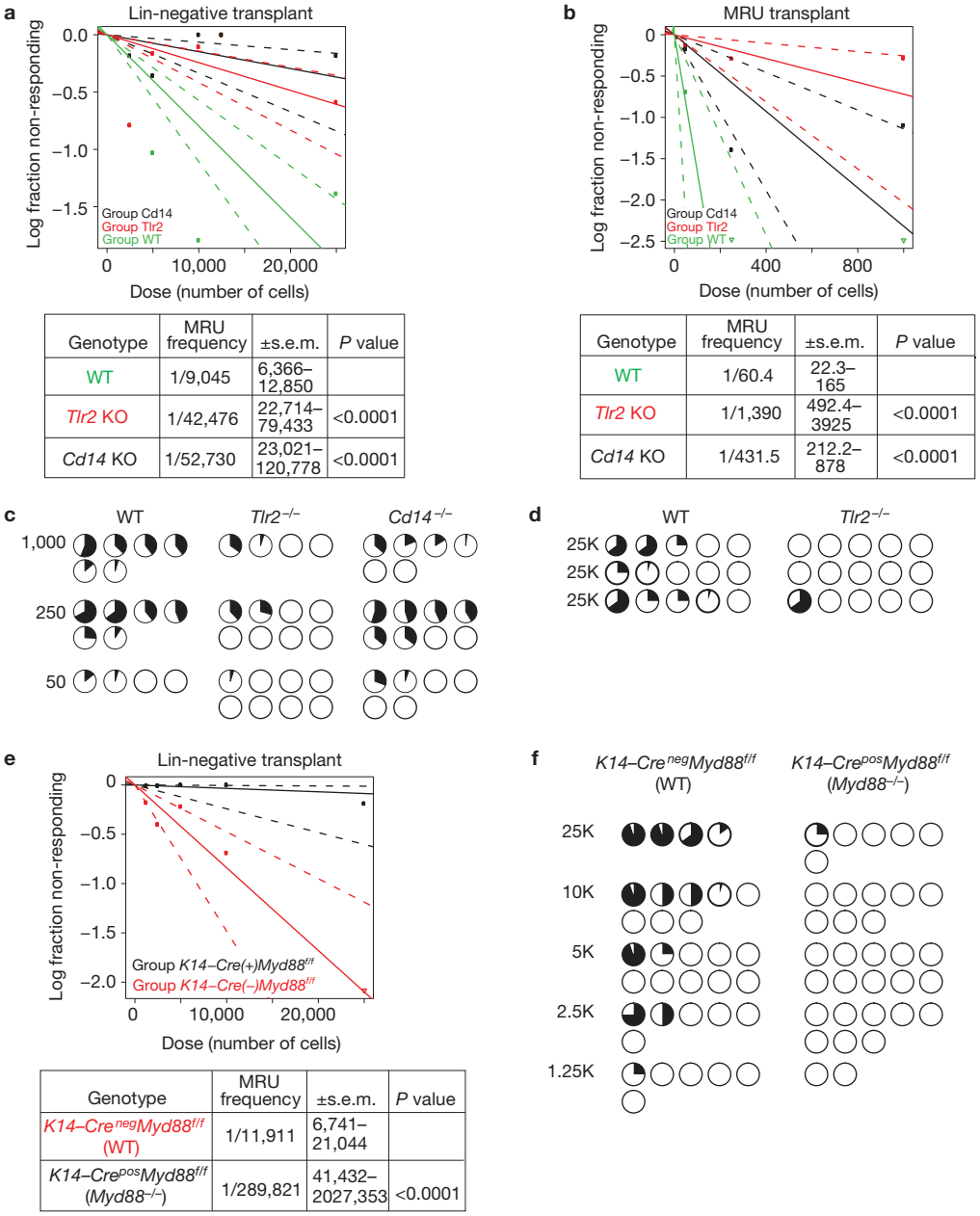

Genotype	MRU frequency	±s.e.m.	*P* value
WT	1/9,045	6,366–12,850	
Tlr2 KO	1/42,476	22,714–79,433	<0.0001
Cd14 KO	1/52,730	23,021–120,778	<0.0001

Genotype	MRU frequency	±s.e.m.	*P* value
WT	1/60.4	22.3–165	
Tlr2 KO	1/1,390	492.4–3925	<0.0001
Cd14 KO	1/431.5	212.2–878	<0.0001

Genotype	MRU frequency	±s.e.m.	*P* value
K14–Cre^{neg}*Myd88*$^{f/f}$ (WT)	1/11,911	6,741–21,044	
K14–Cre^{pos}*Myd88*$^{f/f}$ (*Myd88*$^{-/-}$)	1/289,821	41,432–2027,353	<0.0001

Figure 4 Limiting dilutions of mammary epithelial cells. (**a**) Limiting dilution transplant of *Tlr2*$^{-/-}$ and *Cd14*$^{-/-}$lin^{neg} MECs. ELDA graph and analysis showing stem cell (MRU) frequencies. Data for: WT ($N=75$ samples) pooled from 5+ independent experiments; *Tlr2*$^{-/-}$ ($N=75$ samples) pooled from 5+ independent experiments, $P<0.0001$; *Cd14*$^{-/-}$ ($N=46$ samples) pooled from 4 independent experiments, $P<0.0001$. (**b**,**c**) Limiting dilutions transplant of *Tlr2*$^{-/-}$ and *CD14*$^{-/-}$ sorted MRUs including ELDA graph and analysis of MRU frequencies and pie charts showing mammary tree coverage of the fatpad of individual recipients in each group. Data for WT ($N=16$ samples), *Tlr2*$^{-/-}$ ($N=20$ samples), $P<0.0001$ and *Cd14*$^{-/-}$ ($N=20$ samples), $P<0.0001$, pooled from 3 independent experiments. (**d**) Pie charts for secondary transplants of MECs from primary MRU transplants of WT and *Tlr2*$^{-/-}$ mice. Secondary transplants were done using Lin^{neg} cells (25K, 10–12 weeks after primary transplants of mice from **a**). Data for WT ($N=15$ samples) and *Tlr2*$^{-/-}$ ($N=15$ samples) pooled from 3 independent experiments. Student's unpaired *t*-test for independent samples was used; $P=0.007$. (**e**,**f**) Limiting dilution transplant of *Myd88*-deficient lin^{neg} MECs using *K14–Cre*^{neg} *Myd88*$^{f/f}$ (WT), *K14–Cre*^{pos} *MyD88*$^{f/f}$ (*Myd88*$^{-/-}$) including pie charts showing mammary tree coverage of the fatpad in individual recipients in each group. ELDA graph and analysis showing MRU frequency. Data for WT ($N=34$ samples) and *Myd88*$^{-/-}$ ($N=34$ samples) pooled from 4 independent experiments. $P<0.0001$.

we investigated whether it might play a role in human cancer. Genomic copy number alterations of the TLR2 downstream effectors, IRAK1 and IRAK4, are common; amplifications are found in breast (IRAK1, 23.8%) and colon (IRAK1, 18%; IRAK, 39.7%) cancer (www.broadinstitute.org/tumorscape). In addition, analysis of TLR2 in 482 breast tumours and 240 colon tumours from publicly available data sets (cBio Cancer Genomics Portal and Sanger Catalogue of Somatic Mutations in Cancer) revealed 1 case of a nonsense mutation (R230X) in breast cancer and 4 cases of nonsense mutations (E230X, E283X (2X), E481X) in colon cancer.

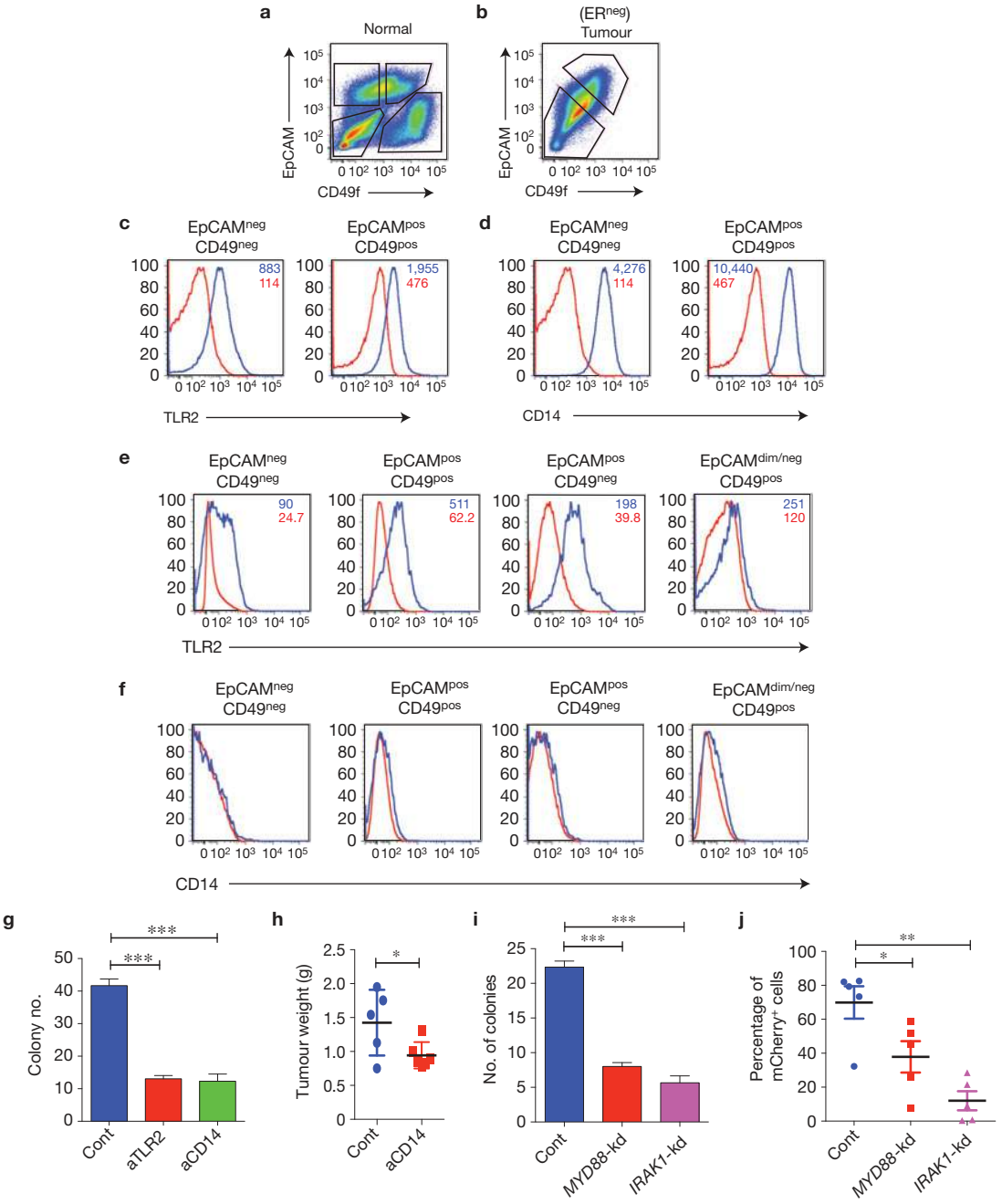

Figure 5 TLR2 expression on human ER^{neg} breast cancer influences *in vitro* colony formation. (**a**,**b**) Representative flow cytometry analysis of normal breast epithelial cells (**a**) and of primary ER^{neg} breast tumours (**b**). (**c**,**d**) Representative histograms for TLR2 (**c**) and CD14 (**d**) of the outlined populations in (**b**). Red: isotype control; blue: TLR2 or CD14 staining. (**e**,**f**) Representative histograms for TLR2 (**e**) and CD14 (**f**) of the outlined populations in **a**. Red: isotype control; blue: TLR2 or CD14 staining. (**a**–**f**) Data are representative of more than 10 independent patient samples. (**g**) *In vitro* colony-forming capacity of a primary ER^{neg} tumour. Neutralizing anti-TLR2 and anti-CD14 blocked clonogenicity; data are shown for one representative tumour of 4 different primary tumours. $N = 3$ samples. $^{***}P < 0.001$. (**h**) Neutralizing anti-CD14 inhibits *in vivo* tumour growth in a breast tumour xenotransplantation model. Data shown are for one representative of 2 experiments with different primary tumours. Control (Cont), $N = 5$ mice; anti-CD14 (aCD14), $N = 5$ mice; $^{*}P = 0.04$. (**i**) Knockdown of *MYD88* or *IRAK1* resulted in decreased clonogenicity in primary ER^{neg} tumour. ($N = 3$ samples); $^{***}P < 0.001$. Data shown are for a representative of 2 different primary tumours. (**j**) *In vivo* effects of *MYD88* or *IRAK1* knockdown in primary ER^{neg} tumour ($N = 5$ mice for each condition). $^{*}P = 0.0425$, $^{**}P = 0.0008$. Data shown are for a representative of 2 different primary tumours. Each group consists of 5 mice. All values in this figure represent mean ± s.d. Student's unpaired *t*-test for independent samples was used.

As IRAK1 and IRAK4 amplifications are common in colon and breast cancer, respectively, we set out to determine the role of the TLR pathway in human breast cancer. Flow cytometry analysis revealed that in contrast to normal human (Fig. 5a) and mouse MECs (Supplementary Fig. 1), which have distinct luminal and basal phenotypes, many human ER^{neg} breast tumours contain

a homogeneous population of EpCAM^{pos}CD49f^{pos} cells (Fig. 5b). Similar to normal murine Ma-CFCs, which contain the highest expression of TLR2 (Fig. 3a) and CD14 (ref. 23; Supplementary Fig. 2d), the EpCAM^{pos}CD49f^{pos} population of ER^{neg} tumour cells also has a high expression of TLR2 and CD14 (Fig. 5c,d). TLR2 and CD14 were also expressed on normal MECs (Fig. 5e,f). To determine whether TLR2 and CD14 are needed for the growth of EpCAM^{pos}CD49f^{pos} cells from human ER^{neg} breast tumours, we cultured these cells *in vitro* on Matrigel, and treated them with a neutralizing antibody against TLR2 or CD14. The TLR2 and CD14 neutralizing antibody blocked colony formation of ER^{neg} tumour cells (Fig. 5g and Supplementary Fig. 5a). Furthermore, a CD14 neutralizing antibody blocked tumour growth of two independent ER^{neg} breast cancer xenografts *in vivo* (Fig. 5h). Short hairpin RNA (shRNA)-mediated knockdown of TLR2 in two breast cell lines similarly decreased clonogenic outgrowth (Supplementary Figs 5b and 6c).

Next, MYD88 and IRAK1, which participate in TLR signalling downstream of TLR2, were investigated. Cells isolated from human breast ER^{neg} xenograft tumours and breast cancer cell lines were treated with shRNAs against MYD88 and IRAK1, then cultured on Matrigel to determine their ability to form colonies *in vitro*. Inhibition of MYD88 and IRAK1 resulted in decreased clonogenicity (Fig. 5i and Supplementary Fig. 5d,e) and decreased NF-κB activity as indicated by *IL-1B* expression (Supplementary Fig. 5f). The MYD88 and IRAK1 shRNAs also resulted in a negative selection in the formation of *in vivo* xenograft tumours derived from ER^{neg} breast cancer cells (Fig. 5j). Together these data support the notion that TLR2 and CD14 are expressed on some ER^{neg} breast cancers and that the TLR2–CD14–MYD88–IRAK1 pathway is important for tumorigenicity.

Finally, because our data suggest that the TLR2 pathway plays an important role in the formation of pre-cancerous polyps/adenomas in the *Apc*$^{min/+}$ mouse model, we wanted to evaluate the role of the TLR2 pathway in human primary tumours. Immunohistochemistry and flow cytometry analysis showed that normal colon epithelial and colon cancer cells express TLR2 (Fig. 6a–c and Supplementary Fig. 6). To ascertain whether TLR2 functions in colon cancer, we cultured primary colon tumours cells *in vitro* on Matrigel and treated the cells with a TLR2 neutralizing antibody. The TLR2 neutralizing antibody blocked colony formation in primary colon cancer (Fig. 6d). Furthermore, we found in a multivariate analysis from two independent data sets that high TLR2 expression is significantly associated with worse overall survival in colon cancer (Fig. 6e). Together, these findings show that the TLR2 pathway is important in murine intestinal tumorigenesis as well as in human colon cancer.

As mutational studies of *Drosophila* TLR (ref. 27) and mammalian TLR4 (ref. 22) showed that truncated TLR mutants can be constitutively active, we assessed whether nonsense mutations found in public data sets of human colon and breast cancers can activate TLR2 signalling. We first examined whether these cancer mutations can lead to the expression of a truncated TLR2 from a downstream alternative start site (M490; Fig. 7a). We generated WT TLR2 (wtTLR2) and mutant TLR2-E283X (ΔTLR2) vectors fused to YFP for easy visualization and transfected them into HEK293T cells. YFP was detected with both the wtTLR2–YFP fusion as well as the ΔTLR2–YFP fusion, showing that the ΔTLR2–YFP mutant was transcribed and translated (Fig. 7b). As TLR2 signals through the NF-κB pathway, we tested whether the deletion mutant could induce activation of NF-κB. Transient expression of ΔTLR2–YFP caused an increased NF-κB activation as compared with wtTLR2–YFP, confirming that this deletion mutant is a gain-of-function mutant leading to constitutive activation of NF-κB (Fig. 7c). In addition, we used CAS9-induced genome editing to create a similar truncated TLR2 gene in HEK293T cells[19,21] (Fig. 7d and Supplementary Fig. 7). This resulted in an increase in expression of *IL-1B* (indicates NF-κB activation), Axin2 and *Lgr5* (suggests an increase in Wnt signalling; Fig. 7e). All of these data suggest that truncated TLR2 can be constitutively active and that the TLR2 nonsense mutations found in human tumour cases can potentially result in active TLR2 signalling.

DISCUSSION

Although previous studies have shown a role for TLR2 and MYD88 in tumour growth and progression[14,39] and a tumour-cell-extrinsic role for TLR2 and MYD88 (refs 6,31), this study suggests cell-intrinsic TLR2–CD14–MYD88 signalling in colon and breast epithelial cells; however, this does not exclude a potential role for cell-extrinsic signalling through the same pathway. The suggested epithelial-cell-intrinsic role is demonstrated by using intestinal- and mammary-specific *MyD88*-deletion mice and by transplanting MECs into WT recipients. All of these data suggest that there is a cell-intrinsic component of TLR2–CD14–MyD88 signalling in epithelial cells.

In MECs, our analysis of mutant mice suggests that the TLR2 pathway is important for normal mammary gland development and the self-renewal property of MRUs. In colon epithelial cells, our data suggest that the TLR2–MYD88 pathway is important in the expansion of the stem and progenitor cell pool during regeneration after injury as demonstrated by the DSS colitis animal model. Hence, TLR2 signalling can potentially play an important role in regulating self-renewal independent of its role in inflammation or in haematopoietic cells[39].

It would be intriguing to know which endogenous TLR2 ligand(s) can activate TLR2 signalling in stem cells. Interestingly, many endogenous TLR2 ligands are secreted by dying cells. Apoptosis is a crucial step during normal mammary development, especially lumen formation[41,43], as well as during intestinal cell differentiation[44]. Furthermore, the intestinal epithelium demonstrates a remarkable capacity for responding to injury or increased apoptosis by upregulating the self-renewal capacity of stem cells. It is possible that TLR2 signalling could play a role in such stem cell plasticity. For example, HMGB1, which is released during apoptosis and cell death, has been shown to induce a TLR2-dependent inflammatory response in haematopoietic cells[45–47]. In addition, we provide evidence that HMGB1 induces epithelial cell clonogenicity, thereby linking apoptosis and TLR2 signalling.

As inflammation in response to pathogens leads to collateral damage and death to normal cells, one could speculate that these ligands simultaneously stimulate innate immune cells and proliferation of normal stem cells to facilitate the repair of the tissue damage induced by the inflammatory response. This increased proliferation would be accompanied by an increased mutation rate, providing a direct molecular link of TLR signalling to inflammation and cancer. In support of this, we show that inactivation of TLR, specifically in intestinal epithelial cells, significantly reduces the development of cancers in an *Apc* mutant mouse model.

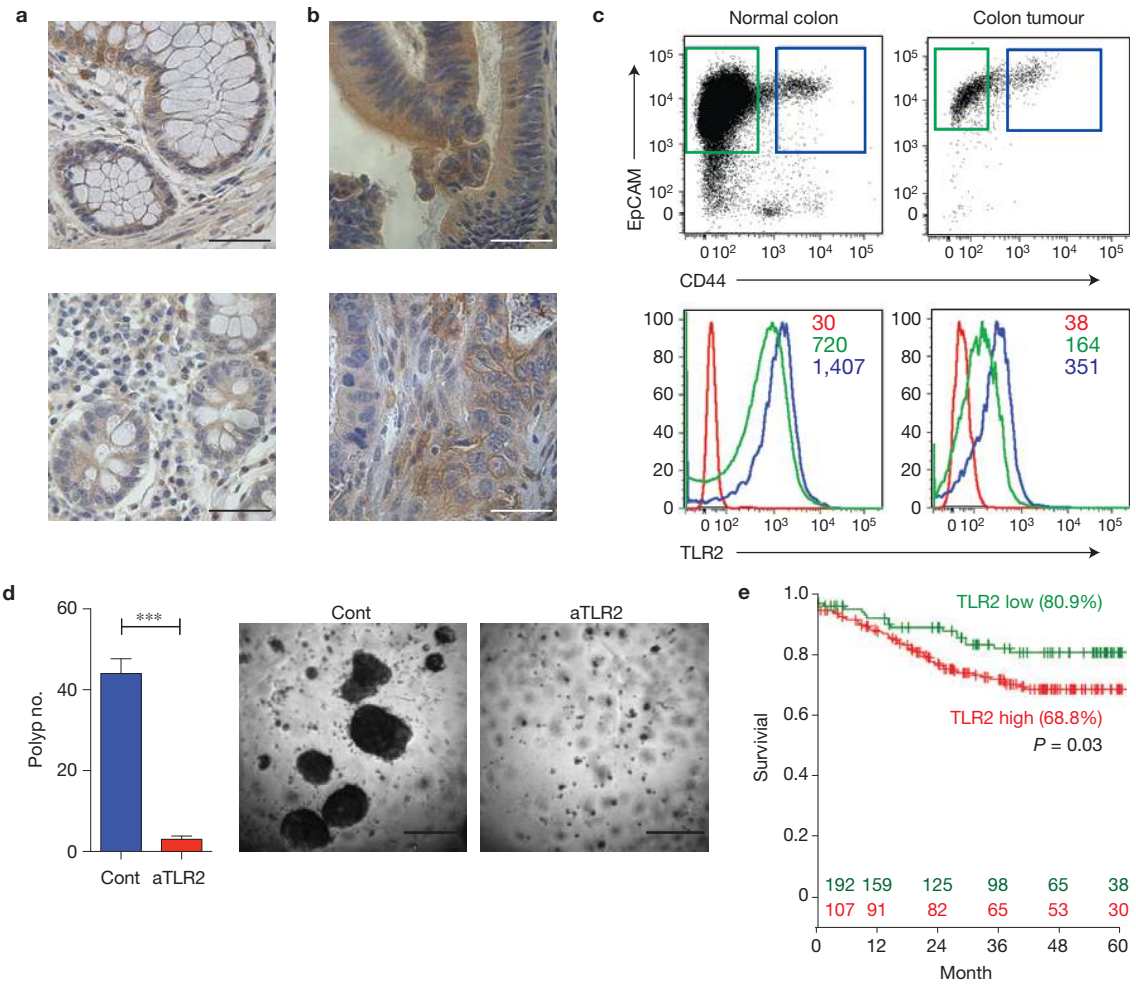

Figure 6 TLR2 expression on colon cancer influences *in vitro* colony formation. (**a**,**b**) Immunohistochemistry for TLR2 in normal colon (**a**) and colon cancer (**b**). Data are representative of more than 10 independent patient samples (scale bar, 50 μm). (**c**) Representative histograms of flow cytometry analysis of a primary colon cancer and normal colon epithelial cells for TLR2; in red: isotype control; in blue: $CD44^{-}$ cells; in green: $CD44^{+}$ cells. Data are representative of 4 independent patient samples. (**d**) *In vitro* colony-forming capacity of a primary colon cancer. Neutralizing anti-TLR2 blocked clonogenicity. $N=3$ independent experiments of one tumour. Data are for one representative tumour of 3 different tumours; $^{***}P$ value is 0.0008. Values represent mean ± s.d. Student's unpaired *t*-test for independent samples was used. (Scale bar, 500 μm.) (**e**) Kaplan–Meier analysis of the probability of overall survival according to TLR2 expression. TLR2 high ($N=107$ patients), TLR2 low ($N=192$ patients); data pooled from 2 independent data sets. $P=0.03$.

Pathways used by normal stem cells are frequently used by cancer cells[49,51]. Several lines of evidence suggest that TLR signalling drives proliferation of at least a subset of cancers. Large-scale sequencing of human tumours has shown that although there are certain genes that are commonly mutated in tumours, there are also a large number of mutations that occur at much lower frequency. A better insight into the role of uncommon genetic variants/mutation will have implications for the detection and management of cancer. This has recently been shown by the finding that rare *PPM1D* mutations lead to a predisposition to develop breast and ovarian cancer[52]. In breast cancer, *IRAK1* is frequently amplified in breast cancer and is in the peak of the amplicon (www.broadinstitute.org/tumorscape), which suggest that activation of the TLR pathway might occur in a significant number of patients. In support of this, our data clearly show that TLR signalling drives proliferation of both colon and ER^{neg} breast cancer cells *in vitro*. In addition, our data demonstrate a low rate of mutations that can result in constitutive TLR2 signalling. Importantly, blocking TLR signalling in an ER^{neg} tumour *in vivo* by a CD14 neutralizing antibody inhibits tumour growth. This demonstrates that the pathway is used by tumours *in vivo*. Recently, NF-κB has been shown to directly activate Wnt signalling, which can potentially lead to tumour initiation[48]. Our data show that in epithelial cells of the intestinal tract and the mammary, TLR2–MYD88 affects the expression of *Wnt* target genes (for example, *Lgr5* and *Cd44*). This potentially explains the reduced tumorigenicity in $Tlr2^{-/-}$ or *Myd88*-deficient MMTV–Wnt1 and $Apc^{min/+}$ models.

ER^{neg} breast cancers have a tendency to relapse and metastasize, and are associated with recurrence, metastasis and a high mortality rate[14,54–56]. The data presented here suggest that there may be a role in targeting the TLR2–MYD88–CD14–IRAK1 signalling pathway to develop potential drugs to treat this subset of breast cancer patients who generally have a poorer prognosis. Different TLRs (for example, TLR2 and TLR4) are potentially active in these tumours but share

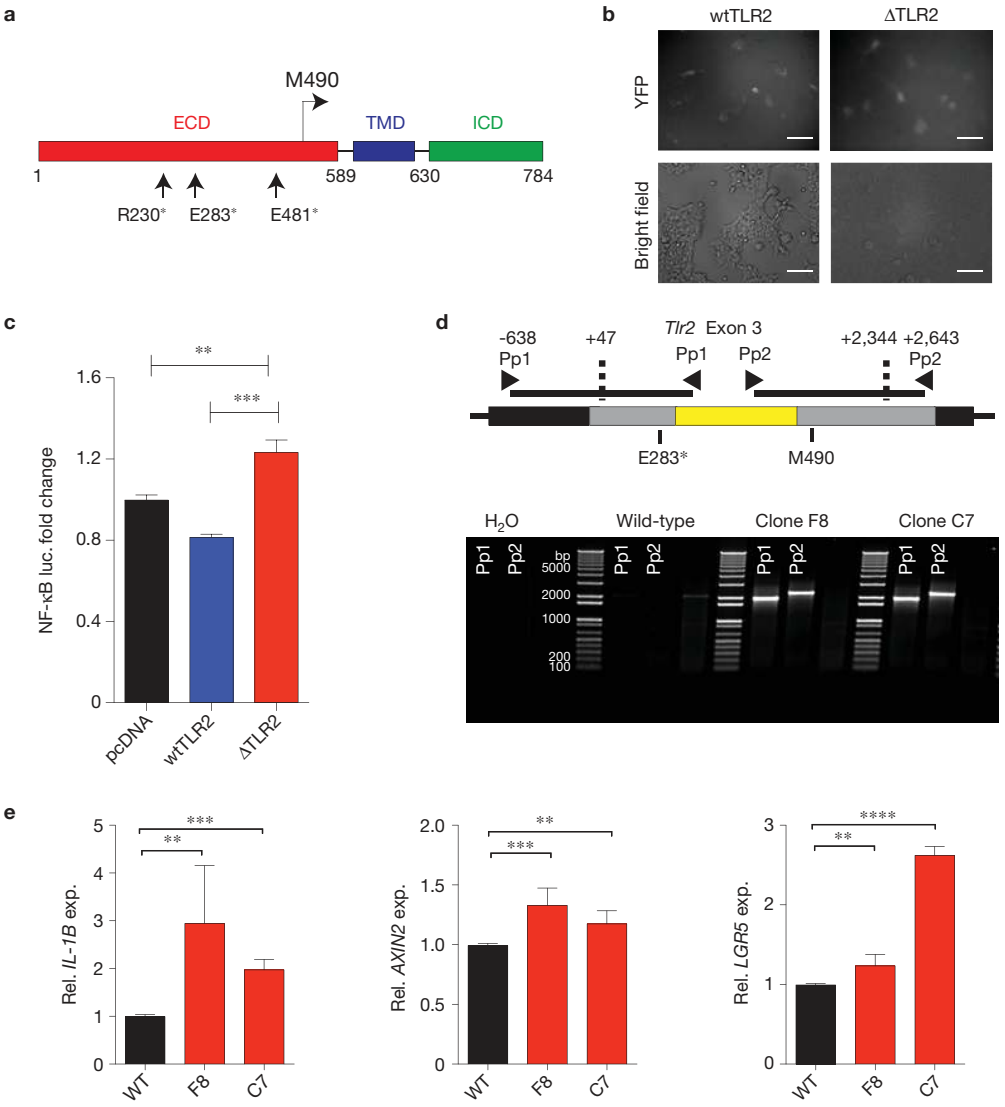

Figure 7 Analysis of TLR2 mutations. (**a**) Structure of the TLR2 gene. Extracellular domain (ECD), transmembrane domain (TMD) and intracellular domain (ICD). The nonsense mutations and the alternative in frame start-site (M490) are shown. (**b**) Protein expression of wtTRL2–YFP and ΔTRL2–YFP mutant as determined by fluorescence of YFP by fluorescence microscopy. (Scale bar, 100 μm.) (**c**) ΔTRL2–YFP mutant constitutively activate NF-κB as determined with an NF-κB-driven luciferase reporter; $N=6$ independent examples per condition; $^{**}P<0.01$; $^{***}P<0.001$. Values represent mean ± s.d. Student's unpaired *t*-test for independent samples was used. (**d**) Strategy of the genome modification using Cas9 to induce double-stranded breaks in the *Tlr2* locus, and template for homology redirected repair (left arm starts at +46 and right arm ends at +2344 with an antisense CMV–Cherry–pA cassette in between. Primer pairs (Pp1 and Pp2) consist of 1 primer specific for the HR construct and 1 specific for the untargeted TLR2 locus. PCR analysis showing insertion of the targeting vector by homologous recombination. (**e**) Real-time qPCR for *IL-1B*, *AXIN2* and *LGR5* on 2 genome-modified clones with genome-edited *Tlr2*. $N=3$ independent experiments; *Il-1b* expression, $^{**}P=0.02$, $^{***}P=0.0001$; *Axin2* expression, $^{**}P=0.01$, $^{***}P=0.003$; *Lgr5* expression, $^{**}P=0.01$; $^{****}P=0.0000001$. Values represent mean ± s.d. Student's unpaired *t*-test for independent samples was used.

common downstream effectors such as MYD88 and the co-receptor CD14. Inhibiting these targets may provide a more generalized inhibition of tumour growth. However, as such inhibitors are likely to also inhibit the pathway in innate immune cells, it is difficult to predict the effects on tumours by concurrent inhibition of the pathway in epithelial cells and innate immune cells. Recent studies demonstrate that blocking tumour cell CD47, which allows tumours to evade the innate immune system, seems to have therapeutic potential in breast cancer[57]. Hence, to preserve an innate immune response against the tumour, a combinatorial therapeutic strategy that combines neutralizing antibodies against CD14 (or IRAK1 kinase inhibitors) with a neutralizing antibody against CD47 may be effective. In this combination, inhibition of TLR signalling could directly inhibit tumour cell growth, whereas inactivation of CD47 could potentially activate an innate immune response against the tumour through a TLR-independent pathway[58]. □

METHODS

Methods and any associated references are available in the online version of the paper.

Note: Supplementary Information is available in the online version of the paper

ACKNOWLEDGEMENTS
This study was supported by the National Institutes of Health (NCI), the Breast Cancer Research Foundation, the Ludwig Institute, The California Institute for Regenerative Medicine and the Department of Defense (DOD). F.A.S. was supported by NWO-Rubicon grant, a fellowship from the Dutch Cancer Society and by a seed grant of the organization My Blue Dots. We thank T.N. Schumacher and M.A. Child for scientific input, S. Sim for her assistance with single-cell PCR assays, P. Lovelace for her assistance with flow cytometry and K. Montgomery for IHC. Some research was performed on a FACS Aria that was purchased using NIH S10 Shared Instrumentation Grant (1S10RR02933801) funds.

AUTHOR CONTRIBUTIONS
F.A.S. and A.H.K. performed, designed and analysed research and wrote the paper; L.J.v.W., S.C., M.Z., S.S.S., I.G., D.J. and M.E.R. performed, designed and analysed research; D.Q. and J.S.L. performed research; J.P.V., T.K., S.R.Q., D.S. and M.v.d.R. designed and analysed research; F.M.D. and G.S. provided critical reagents; M.F.C. designed research and wrote paper.

COMPETING FINANCIAL INTERESTS
The authors declare no competing financial interests.

Published online at www.nature.com/doifinder/10.1038/ncb3058
Reprints and permissions information is available online at www.nature.com/reprints

1. Metcalfe, C., Kljavin, N. M., Ybarra, R. & de Sauvage, F. J. Stem cells are indispensable for radiation-induced intestinal regeneration. *Cell Stem Cell* **14,** 149–159 (2014).
2. Yu, L., Wang, L. & Chen, S. Endogenous toll-like receptor ligands and their biological significance. *J. Cell. Mol. Med.* **14,** 2592–2603 (2010).
3. Akira, S., Uematsu, S. & Takeuchi, O. Pathogen recognition and innate immunity. *Cell* **124,** 783–801 (2006).
4. West, X. Z. *et al.* Oxidative stress induces angiogenesis by activating TLR2 with novel endogenous ligands. *Nature* **467,** 972–976 (2010).
5. Park, J. S. High mobility group box 1 protein interacts with multiple Toll-like receptors. *Am. J. Physiol. Cell Physiol.* **290,** C917–C924 (2005).
6. Kim, S. *et al.* Carcinoma-produced factors activate myeloid cells through TLR2 to stimulate metastasis. *Nature* **457,** 102–106 (2009).
7. Yang, R-B. *et al.* Toll-like receptor-2 mediates lipopolysaccharide-induced cellular signalling. *Nature* **395,** 284–288 (1998).
8. Lee, M. S. & Kim, Y-J. Signaling pathways downstream of pattern-recognition receptors and their cross talk. *Annu. Rev. Biochem.* **76,** 447–480 (2007).
9. Wright, S. D., Ramos, R. A., Tobias, P. S., Ulevitch, R. J. & Mathison, J. C. CD14, a receptor for complexes of lipopolysaccharide (LPS) and LPS binding protein. *Science* **249,** 1431–1433 (1990).
10. Clevers, H. At the crossroads of inflammation and cancer. *Cell* **118,** 671–674 (2004).
11. Rakoff-Nahoum, S. & Medzhitov, R. Toll-like receptors and cancer. *Nat. Rev. Cancer* **9,** 57–63 (2009).
12. Coussens, L. M. & Werb, Z. Inflammation and cancer. *Nature* **420,** 860–867 (2002).
13. Balkwill, F. & Mantovani, A. Inflammation and cancer: back to Virchow? *Lancet* **357,** 539–545 (2001).
14. Rakoff-Nahoum, S. & Medzhitov, R. Regulation of spontaneous intestinal tumorigenesis through the adaptor protein MyD88. *Science* **317,** 124–127 (2007).
15. Takeda, K., Kaisho, T. & Akira, S. Toll-like receptors. *Annu. Rev. Immunol.* **21,** 335–376 (2003).
16. Ngo, V. N. *et al.* Oncogenically active MYD88 mutations in human lymphoma. *Nature* **470,** 115–119 (2011).
17. Puente, X. S. *et al.* Whole-genome sequencing identifies recurrent mutations in chronic lymphocytic leukaemia. *Nature* **475,** 101–105 (2011).
18. Pietersen, A. M. *et al.* Bmi1 regulates stem cells and proliferation and differentiation of committed cells in mammary epithelium. *Curr. Biol.* **18,** 1094–1099 (2008).
19. Cong, L. *et al.* Multiplex genome engineering using CRISPR/Cas systems. *Science* **339,** 819–823 (2013).
20. Uemura, N. *et al. Helicobacter pylori* infection and the development of gastric cancer. *N. Engl. J. Med.* **345,** 784–789 (2001).
21. Mali, P. *et al.* RNA-guided human genome engineering via Cas9. *Science* **339,** 823–826 (2013).
22. Medzhitov, R., Preston-Hurlburt, P. & Janeway, C. A. A human homologue of the *Drosophila* Toll protein signals activation of adaptive immunity. *Nature* **388,** 394–397 (1997).
23. Asselin-Labat, M-L. *et al.* Gata-3 negatively regulates the tumor-initiating capacity of mammary luminal progenitor cells and targets the putative tumor suppressor Caspase-14. *Mol. Cell Biol.* **31,** 4609–4622 (2011).
24. Shackleton, M. *et al.* Generation of a functional mammary gland from a single stem cell. *Nature* **439,** 84–88 (2006).
25. Stingl, J. *et al.* Purification and unique properties of mammary epithelial stem cells. *Nature* **439,** 993–997 (2006).
26. Kordon, E. C. & Smith, G. H. An entire functional mammary gland may comprise the progeny from a single cell. *Development* **125,** 1921–1930 (1998).
27. Schneider, D. S., Hudson, K. L., Lin, T. Y. & Anderson, K. V. Dominant and recessive mutations define functional domains of Toll, a transmembrane protein required for dorsal-ventral polarity in the *Drosophila* embryo. *Genes Dev.* **5,** 797–807 (1991).
28. Keymeulen, A. V. *et al.* Distinct stem cells contribute to mammary gland development and maintenance. *Nature* **479,** 189–193 (2011).
29. Rios, A. C., Fu, N. Y., Lindeman, G. J. & Visvader, J. E. *In situ* identification of bipotent stem cells in the mammary gland. *Nature* **506,** 322–327 (2014).
30. Plaks, V. *et al.* Lgr5-expressing cells are sufficient and necessary for postnatal mammary gland organogenesis. *Cell Rep.* **3,** 70–78 (2013).
31. Grivennikov, S. I. *et al.* Adenoma-linked barrier defects and microbial products drive IL-23/IL-17-mediated tumour growth. *Nature* **491,** 254–258 (2012).
32. Sangiorgi, E. & Capecchi, M. R. Bmi1 is expressed *in vivo* in intestinal stem cells. *Nat. Genet.* **40,** 915–920 (2008).
33. Tian, H. *et al.* A reserve stem cell population in small intestine renders Lgr5-positive cells dispensable. *Nature* **478,** 255–259 (2011).
34. Montgomery, R. K. *et al.* Mouse telomerase reverse transcriptase (mTert) expression marks slowly cycling intestinal stem cells. *Proc. Natl Acad. Sci. USA* **108,** 179–184 (2011).
35. Takeda, N. *et al.* Interconversion between intestinal stem cell populations in distinct niches. *Science* **334,** 1420–1424 (2011).
36. Powell, A. E. *et al.* The Pan-ErbB negative regulator Lrig1 is an intestinal stem cell marker that functions as a tumor suppressor. *Cell* **149,** 146–158 (2012).
37. Muñoz, J. *et al.* The Lgr5 intestinal stem cell signature: robust expression of proposed quiescent '+4' cell markers. *EMBO J.* **31,** 3079–3091 (2012).
38. Barker, N. *et al.* Identification of stem cells in small intestine and colon by marker gene Lgr5. *Nature* **449,** 1003–1007 (2007).
39. Tye, H. *et al.* STAT3-driven upregulation of TLR2 promotes gastric tumorigenesis independent of tumor inflammation. *Cancer Cell* **22,** 466–478 (2012).
40. Rakoff-Nahoum, S., Paglino, J., Eslami-Varzaneh, F., Edberg, S. & Medzhitov, R. Recognition of commensal microflora by toll-like receptors is required for intestinal homeostasis. *Cell* **118,** 229–241 (2004).
41. Humphreys, R. C. *et al.* Apoptosis in the terminal endbud of the murine mammary gland: a mechanism of ductal morphogenesis. *Development* **122,** 4013–4022 (1996).
42. Kitajima, S., Takuma, S. & Morimoto, M. Changes in colonic mucosal permeability in mouse colitis induced with dextran sulfate sodium. *Exp. Anim.* **48,** 137–143 (1999).
43. Mailleux, A. *et al.* BIM regulates apoptosis during mammary ductal morphogenesis, and its absence reveals alternative cell death mechanisms. *Dev. Cell* **12,** 221–234 (2007).
44. Hall, P. A., Coates, P. J., Ansari, B. & Hopwood, D. Regulation of cell number in the mammalian gastrointestinal tract: the importance of apoptosis. *J. Cell Sci.* **107,** 3569–3577 (1994).
45. Bianchi, M. E. & Manfredi, A. A. High-mobility group box 1 (HMGB1) protein at the crossroads between innate and adaptive immunity. *Immunol. Rev.* **220,** 35–46 (2007).
46. Park, J. S. *et al.* Involvement of toll-like receptors 2 and 4 in cellular activation by high mobility group box 1 protein. *J. Biol. Chem.* **279,** 7370–7377 (2004).
47. Urbonaviciute, V. *et al.* Induction of inflammatory and immune responses by HMGB1-nucleosome complexes: implications for the pathogenesis of SLE. *J. Exp. Med.* **205,** 3007–3018 (2008).
48. Schwitalla, S. *et al.* Intestinal tumorigenesis initiated by dedifferentiation and acquisition of stem-cell-like properties. *Cell* **152,** 25–38 (2012).
49. Reya, T., Morrison, S. J., Clarke, M. F. & Weissman, I. L. Stem cells, cancer, and cancer stem cells. *Nature* **414,** 105–111 (2001).
50. Barker, N. *et al.* Crypt stem cells as the cells-of-origin of intestinal cancer. *Nature* **457,** 608–611 (2009).
51. Shackleton, M., Quintana, E., Fearon, E. R. & Morrison, S. J. Heterogeneity in cancer: cancer stem cells versus clonal evolution. *Cell* **138,** 822–829 (2009).
52. Ruark, E. *et al.* Mosaic PPM1D mutations are associated with predisposition to breast and ovarian cancer. *Nature* **493,** 406–410 (2012).
53. Schepers, A. G. *et al.* Lineage tracing reveals Lgr5+ stem cell activity in mouse intestinal adenomas. *Science* **337,** 730–735 (2012).
54. Dent, R. *et al.* Pattern of metastatic spread in triple-negative breast cancer. *Breast Cancer Res. Treat.* **115,** 423–428 (2009).
55. Bauer, K. R., Brown, M., Cress, R. D., Parise, C. A. & Caggiano, V. Descriptive analysis of estrogen receptor (ER)-negative, progesterone receptor (PR)-negative, and HER2-negative invasive breast cancer, the so-called triple-negative phenotype: a population-based study from the California cancer Registry. *Cancer* **109,** 1721–1728 (2007).
56. Carey, L. A. *et al.* Race, breast cancer subtypes, and survival in the Carolina Breast Cancer Study. *JAMA* **295,** 2492–2502 (2006).
57. Willingham, S. B. *et al.* The CD47-signal regulatory protein alpha (SIRPa) interaction is a therapeutic target for human solid tumors. *Proc. Natl Acad. Sci. USA* **109,** 6662–6667 (2012).
58. Chao, M. P. *et al.* Calreticulin is the dominant pro-phagocytic signal on multiple human cancers and is counterbalanced by CD47. *Sci. Transl. Med.* **2,** 63ra94 (2010).
59. Asselin-Labat, M-L. *et al.* Gata-3 is an essential regulator of mammary-gland morphogenesis and luminal-cell differentiation. *Nat. Cell Biol.* **9,** 201–209 (2007).

DOI: 10.1038/ncb3058

METHODS

Mice. *Tlr2*$^{-/-}$ mice (B6.129-*Tlr2*^{tm1Kir}/J), *Cd14*$^{-/-}$ mice (B6.129S-*Cd14tm1Frm*/J), *Tlr4*$^{-/-}$ mice (B6.B10ScN-*Tlr4*$^{lps-del}$/JthJ), *Il-1r1*$^{-/-}$ mice (B6.129S7-*Il-1r1*^{tm1Imx}/J), *Il-18r1*$^{-/-}$ mice (B6.129P2-*Il-18r1*^{tm1AKi}/J), *Myd88*$^{-/-}$ mice (B6.129P2(SJL)-*Myd88*$^{tm1.1Defr}$/J), *Myd88*^{flox} mice (B6.129P2(SJL)-*Myd88*^{tm1Defr}/J), *K14–Cre* transgenic mice (Tg(KRT14–cre)1Amc/J), *Apc*^{min} mice (cBL/6J-*ApcMin*/J), FVB.Cg-Tg(Wnt1)1Hev/J, C57BL/6-TgN(ACTbEGFP)1Osb (pCx-GFP) and *Nod/Scid/Il2r*$^{-/-}$ (NSG) mice (NOD.Cg-Prkdc^{scid} IL2Rg^{tm1Wjl}/SzJ) were purchased from the Jackson Laboratory. *Villin–Cre*^{ERT2} (refs 60) was previously described. *K14–Cre* transgenic mice were on a mixed background and were crossed to mice with a C57BL/6J background for 3 generations. Recipient mice in the transplant assays for wild-type, *Tlr2*$^{-/-}$ and *Cd14*$^{-/-}$ cells were C57Bl/6J mice and for the *K14–Cre Myd88*$^{f/f}$ mice we used NSG mice. All mice used for this study were maintained at the Stanford Animal Facility in accordance with the guidelines of the animal care use committee.

Preparation of single-cell suspensions of tissues. Mice were euthanized and all fat pads surgically resected. Tissue was digested in DMEM/F12 for 2 h, and then processed as previously described[25,60,61]. Briefly, mechanically dissociated mammary glands were treated for two hours with collagenase and hyaluronidase (StemCell Technologies) followed by lysis of red blood cells in ACK (NH4CL), followed by 1–2 min treatment with pre-warmed 0.25% trypsin EDTA (Invitrogen), followed by prewarmed dispase (StemCell Technologies) plus DNaseI (Sigma) for 2 min, and filtration through a 70 μm mesh and washed with flow cytometry buffer (HBBS, 2% FCS, PSA). Single-cell samples of murine colon and small intestine were prepared as described previously[16,61].

For human samples, informed consent was obtained after the approval of protocols by the Stanford University and City of Hope Institutional Review Boards. Human breast specimens, and primary or xenograft tumours were mechanically dissociated into >1–2 mm^3 pieces with a razor blade and digested at 37 °C with collagenase and hyaluronidase, in Advanced DMEM/F12 (Invitrogen) with 2 mM Glutamax (Invitrogen), 120 μg ml^{-1} penicillin, 100 μg ml^{-1} streptomycin, 0.25 μg ml^{-1} amphotericin-B (PSA) and incubated for 4–12 h. At the end of the incubation, cells were treated with ACK to lyse the red blood cells followed by a short incubation in dispase and DNaseI. Cells were filtered through a 70 μm nylon mesh and washed with flow cytometry buffer (HBBS, 2% FCS, PSA). Preparation of human colon tumours was performed as described previously[62,63].

DSS-induced colitis. Colitis was induced by 1.5% (w/v) dextran sodium sulphate (DSS; relative molecular mass 36,000–50,000; MP Biochemicals) added to the drinking water for 7 days. Colons were collected for histology or experiment at day 9 to day 11.

***In vivo* transplants.** For mouse transplants, double-sorted live lin^{neg} cells (CD45^{neg}CD31^{neg}TER119^{neg}DAPI^{neg}) or MRU population (Lin^{neg}CD24^{dim}CD49f^{high}) was collected in staining media and resuspended with 50% Matrigel (BD Biosciences). Per transplant 10 μl was injected into cleared fat pads of weaning-age mice (21–28 days), of indicated genotype, as previously described[25]. All transplants were allowed to grow for 6–10 weeks before analysis.

Tumour cell engraftment and treatment. Human tumour cells were suspended in staining media containing 50% Matrigel and injected into the fourth abdominal fat pad by subcutaneous injection at the base of the nipple of female NSG mice. Two weeks after tumour injection mice received 100 mg anti-CD14 (clone 60bca from ATCC) every other day until the end of the experiment. The experiment was performed twice with 5 mice per group.

***In vitro* colony-forming assays.** For the human and mouse 3D *in vitro* colony assay, 96-well ultralow attachment round-bottom plates (BD) were prepared with a feeder layer of irradiated L-WNT3a cells mixed with 40 μl of growth factor reduced-Matrigel (BD) per well. Cells were re-suspended in media and transferred onto the solidified Matrigel mix. Medium used to culture the human cells is as follows: advanced Dulbecco's modified Eagle medium/F12 (Invitrogen), 10% FBS, 2.5% growth factor-reduced Matrigel (BD), 10 μM Y-27632 (sigma), 10 ng ml^{-1} EGF (R&D), 100 ng ml^{-1} Noggin (R&D), 250 ng ml^{-1} RSPO-I (R&D), 1X B27 (Invitrogen), 1X N2 (Invitrogen) 120 μg ml^{-1} penicillin and 100 μg ml^{-1} streptomycin (P/S). Mouse 2D *in vitro* colony assay cells were cultured in Epicult B medium (StemCell Technologies) with 5% serum in the presence of 13,000 cm^2 irradiated NIH-3T3 cells. After 24–48 h, the medium was replaced with serum-free Epicult B, and colonies were counted 7 days later. Anti-TLR2 antibodies were clone T2.5 (10 μg ml^{-1}; eBioscience catalogue number 14-9024-82) and TL2.1 (10 μg ml^{-1}; Biolegend catalogue number 309710). Purified CD14 antibody hybridoma clone 60bca (10 μg ml^{-1}; ATCC catalogue number HB-247) was used for *in vitro* assays. TLR2 ligands: Pam3CSK4 (25 μg ml^{-1}, TLR1/2, Imgenex), Malp-2 (50 ng ml^{-1}, TLR2/6, Imgenex), HMGB1 (50 ng ml^{-1}, TLR2, Sigma-Adrich). HT29, MDA-MB-231, MCF7, MDA-MB-468 and 293T cells were cultured with DMEM supplemented with 10% fetal bovine serum, 100 U penicillin and 100 μg ml^{-1} streptomycin.

Flow cytometry. To reduce nonspecific binding, cells suspended in staining buffer were blocked on ice for 10 min with rat IgG (Sigma) 10 mg ml^{-1} at 1:1,000. Cells were then stained, in the dark, on ice for 30–60 min with optimal antibody concentrations, which were determined by titration experiments. Mouse antibodies include CD45–biotin (clone 30-F11, BD catalogue number 553078); 1 μg ml^{-1}, TER119–biotin (clone TER-119, BD catalogue number 553672) ; 1 μg ml^{-1}, CD31–biotin (clone 390, BD catalogue number 558737); 1 μg ml^{-1}, CD24–Fitc (clone M1/69, eBioscience catalogue number 11-0242-85); 0.5 μg ml^{-1}, TLR2 PeCy7 (clone T2.5, eBioscience catalogue number 25-9024-80); 2 μg ml^{-1}, EpCAM–APC–Cy7 (clone G8.8, Biolegend catalogue number 118218); 1 μg ml^{-1}, TLR4 PeCy7 (clone SA15-21, Biolegend catalogue number 145408); 1 μg ml^{-1}, IL-18R1 Alexa Fluor 647 (clone BG, Biolegend catalogue number 132903); 1 μg ml^{-1}, CD49f–APC (clone GoH3, Biolegend catalogue number 313615); 1 μg ml^{-1}, CD61 PE (clone 2C9.G2, Biolegend catalogue number 104308); 2 μg ml^{-1}, CD14 Apc–Cy7 (clone Sa14-2, Biolegend catalogue number 123318); 1 μg ml^{-1}, streptavidin APC–Cy7 (Biolegend catalogue number 405208); 1 μg ml^{-1} and streptavidin PacificBlue (Invitrogen catalogue number S-11222); 1 μg ml^{-1}. Lineage cells consist of CD45-, TER119- and CD31-positive cells in mouse. Human antibodies used include: EpCAM–Alexa Fluor 488 (clone 9C4, Biolegend catalogue number); 1 μg ml^{-1}, CD49f–APC (clone GoH3, Biolegend catalogue number); 1 μg ml^{-1}, CD14 Apc–Cy7 (clone M5E2, Biolegend catalogue number); 1 μg ml^{-1}, CD10 PeCy7/Apc–Cy7 (clone H110a, Biolegend catalogue number); 1 μg ml^{-1}, H-2Kd biotin/Pacific Blue (clone SF1-1.1, Biolegend catalogue number); 1 μg ml^{-1}, TLR2 PeCy7 (clone T2.5, eBioscience catalogue number); 2 μg ml^{-1}, CD31 biotin (clone WM59, BD Biosciences catalogue number); 1 μg ml^{-1}, CD45 biotin (clone HI30, BD Biosciences catalogue number); 1 μg ml^{-1}, IL-1R1 Alexa Fluor 647 (clone 35F5, BD Biosciences catalogue number); 1 μg ml^{-1} from BD Biosciences. In primary human tissue lineage cells consist of cells positive for CD45 and CD31; in xenograft lineage cells consist of H-2Kd-positive cells. Flow cytometry was performed with a 100 μm nozzle on a BD Flow cytometry Aria II with Flow cytometry Diva software. Data analysis was performed using Flowjo. For all experiments, side scatter and forward scatter profiles (area and width) were used to eliminate debris and cell doublets. Dead cells were eliminated by excluding 4′,6-diamidino-2-phenylindole (DAPI)-positive cells (Molecular Probes).

Plasmids. Sequences for human MyD88 shRNA1, IRAK1 shRNA1 and IRAK1 shRNA4 were obtained from L. M. Staudt (NCI, NIH, USA)[16,64] and cloned into pSUPER. The H1-shRNA cassette (EcoR1–Xho1) was sub-cloned into pCDH1 (EcoR1–Sal1) upstream of EF1a–Cherry. Lentiviral constructs against human TLR2 were purchased from Sigma, and included pLKO.1 puro vector (no. 1 TRCN0000057021 and no. 2 TRCN0000057019). shRNA-pLKO.1-puro control was used a negative control. Lenti-viruses were produced as described previously[63]. pcDNA3 TLR2–YFP (Addgene plasmid 13016) was used for PCR-based mutagenesis to obtain pcDNA3 ΔTLR2–YFP. First PCR: T7 FW primer plus ΔTLR2 Rev (5′-CAGTCATCAAAC TATAATTCTAACAATCC-3′) and TLR2 WT(1705-5′-GGGATGGAGAGTCAC ACAGG-3′)Rev plus ΔTLR2 FW (5′-GGATTGTTAGAATTATAGTTTGATGA CTG-3′); second PCR: T7 FW primer and TLR2 WT(1705)Rev. PCR product was digested with BamH1 and Ecor1 and cloned into pcDNA3 TLR2–YFP and was subsequently sequenced thoroughly. Phusion high-fidelity DNA polymerase (NEB) was used to perform the TLR2-mutation-based PCR.

The PX459 (pSpCAS(BB)-2A-Puro; ref. 65), obtained from Addgene, was used to clone in the sgRNA seq (5′-GGCCTAACAATTGCAAAGGT-3′). Homologous recombination cassette was ordered as a gBlock from IDT; TLR2 locus from +47 to +2344 (exon 3) was cloned using TopoTA cloning kit (Invitrogen). CMV–Cherry–pA was cloned in the Hpa1 site in the anti-sense orientation as determined by sequencing. Primer pairs: Pp1 FW 5′-CTTGGTCTGCCTCGAGT TTC-3′; Pp1 Rev 5′-GAAAGTCCCGTTGATTTTGG-3′; Pp2 FW 5′-CCCCGTA ATGCAGAAGAAGA-3′; Pp2 Rev 5′-GCAACCAATTCCCTTGGATA-3′.

Luciferase reporter assay. HEK293T cells were seeded a day before transfection. All transfections were carried out with Fugene 6 (Promega) according to the manufacturer's instructions. Cells were transfected with NF-κB luciferase expression construct (Promega), pRL-TK *Renilla* luciferase vector (Promega) plus pcDNA3 TLR2–YFP, pcDNA3 ΔTLR2–YFP or pcDNA3 empty control. Luciferase activities were measured using the Dual-Luciferase Reporter Assay System (Promega) and normalized to *Renilla* luciferase activity. Three independent samples were used in triplicate for each experiment. Data are from two independent experiments.

Statistical analysis. Differences between groups were analysed using unpaired Student's *t*-tests. Error bars represent standard deviations (±s.d.). For mouse

survival curves, differences between curves were analysed using the log-rank (Mantel–Cox) test. For limiting dilution analyses, the frequency of mammary repopulating units was calculated using ELDA software[64]. Expected frequencies are reported, as well as the 95% confidence intervals (lower and upper values are indicated). No statistical method was used to predetermine sample size, experiments were not randomized and investigators were not blinded to allocation during experiments. Investigators were blinded when assessing the outcome of animal experiments (animals had only an ear tag no. for identification) during: pathology assessment of DSS-treated colons, and flow cytometry analysis of different groups of treated mice.

Single-cell gene expression. This was performed as described previously[25,60,61]. In short, double-sorted single cells were sorted into individual wells of 96-well plates containing 5 µl lysis buffer (CellsDirect qRT-PCR mix; Invitrogen) and 2U SuperaseIn. After reverse transcription and pre-amplification using multiplexed PCR, reactions were loaded (Hamilton StarLET pipetting robot) on a Fluidigm microfluidic chip. The microfluidic chips were run on the BioMark real-time PCR reader (Fluidigm), and loaded chips underwent thermocycling and fluorescent quantification according to the manufacturer's instructions. Positive or negative associations among pairs of genes were tested by Spearman correlation, and P values were calculated using $n = 10{,}000$ permutations. The following TaqMan assays (Applied Biosystems) were used: Lgr5, Mm00438890_m1; Gata3, Mm00484683_m1; Krt5, Mm00503549_m1; Krt14, Mm00516870_mH; CD44, Mm01277161_m1; Actb, Mm00607939_s1; Trp53, Mm01731287_m1; Krt17, Mm01306857_mH; TLR2, Mm00442346_m1 ;MyD88, Mm0044338; Krt9, Mm01701806_m1.

The following (intron spanning) primers were used for quantitative real-time PCR using SYBR green: Axin2 FW 5′-CTCCCCACCTTGAATGAAGA-3′; Axin2 Rev 5′-TGGCTGGTGCAAAGACATAG-3′; LGR5 FW 5′-CTTCCAACCTCAGC GTCTTC-3′; LGFR5 Rev 5′-TTTCCCGCAAGACGTAACTC-3′; β-actin FW 5′-GG ATGCAGAAGGAGATCACTG-3′; β-actin Rev 5′-CGATCCACACGGAGTACT TG-3′; IL-1B FW 5′-AGCTGATGGCCTAAACAGA-3′; IL-1B Rev 5′-GCATCTT CCTCAGCTTGTCC-3′; TLR2 FW 5′-GGCGTTCTCTCAGGTGACTG-3′; TLR2 Rev 5′-CTTCCTTGGAGAGGCTGATG-3′; MYD88 FW 5′-TTGAGGAGGATTG CCAAAAG-3′; MYD88 Rev 5′-CATCTCCTGCACAAACTGGA-3′; IRAK1 FW 5′-CTCTGACCAGCCAAGGTCTC-3′; IRAK1 Rev 5′-GCCCGAGGAGTACAT CAAGA-3′.

60. el Marjou, F. *et al*. Tissue-specific and inducible Cre-mediated recombination in the gut epithelium. *Genesis* **39,** 186–193 (2004).
61. Rothenberg, M. E. *et al*. Identification of a cKit(+) colonic crypt base secretory cell that supports Lgr5(+) stem cells in mice. *Gastroenterology* **142,** 1195–1205.e6 (2012).
62. Dalerba, P. *et al*. Phenotypic characterization of human colorectal cancer stem cells. *Proc. Natl Acad. Sci. USA* **104,** 10158–10163 (2007).
63. Shimono, Y. *et al*. Downregulation of miRNA-200c links breast cancer stem cells with normal stem cells. *Cell* **138,** 592–603 (2009).
64. Hu, Y. & Smyth, G. K. ELDA: extreme limiting dilution analysis for comparing depleted and enriched populations in stem cell and other assays. *J. Immunol. Methods* **347,** 70–78 (2009).
65. Ran, F. A. *et al*. Genome engineering using the CRISPR-Cas9 system. *Nat. Protoc.* **8,** 2281–2308 (2013).

nature cell biology

DOI: 10.1038/ncb3058

TLR2 and MyD88 expression in murine mammary epithelial subpopulations.

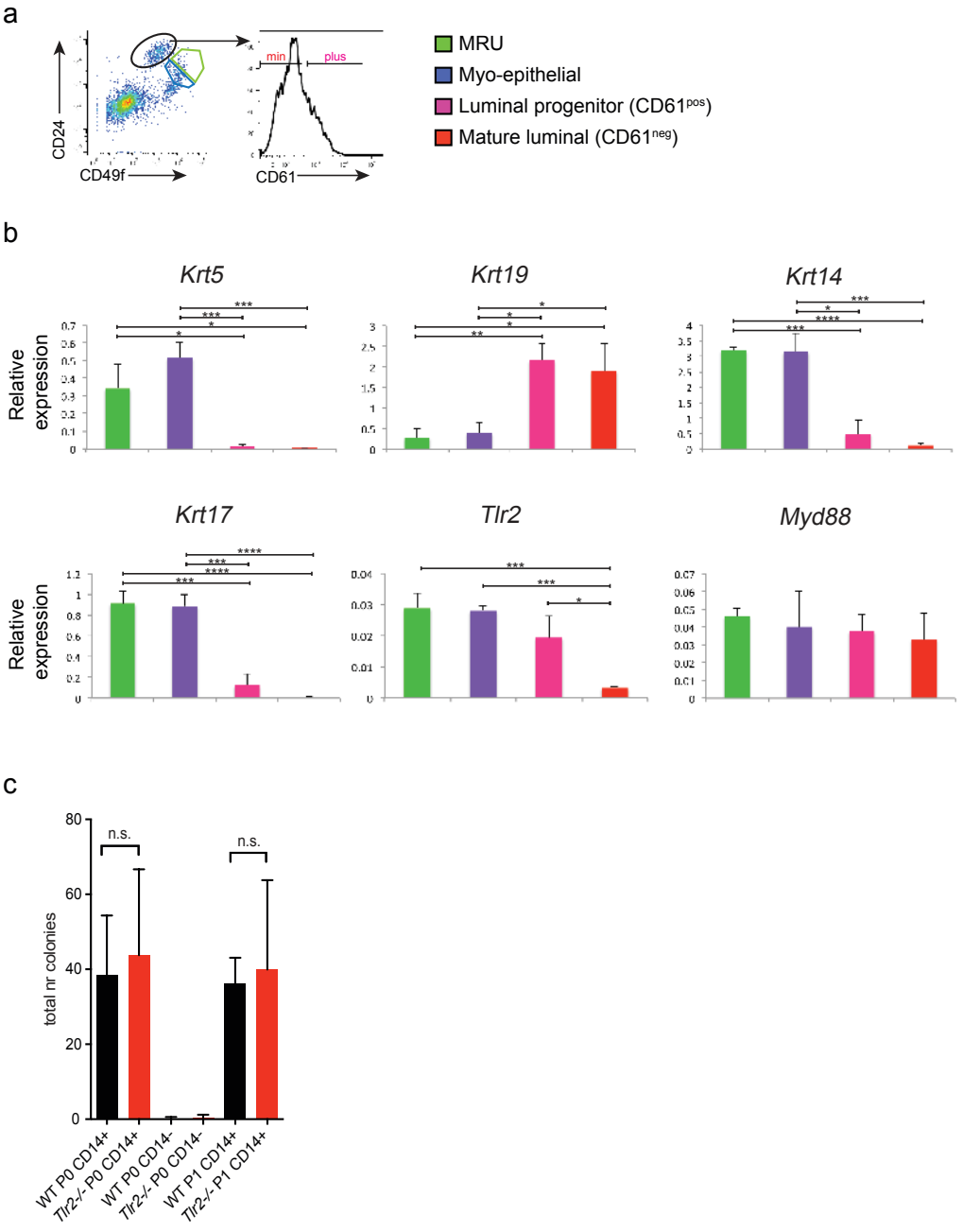

Supplementary Figure 1 TLR2 and MyD88 expression in murine mammary epithelial subpopulations. **(a)** Representative FACS dot plot and histogram of CD24, CD49f and CD61. Data are representative of 6 mice. (**b**) Quantitative rt-PCR on MEC populations as indicated in a. Basal markers: Krt5, Krt14, Krt17; Luminal marker: Krt19; N=3 mice; *, P<0.05; **, P<0.01; ***, P<0.005; ****, P<0.001. Error bars represent S.E.M. One-tail unpaired t-test analysis was used. (**c**) Ma-CFCs were sorted based on expression of $CD24^{high}CD49f^{low/neg}$ luminal phenotype in combination with CD14. 200 cells luminal cells sorted for $CD14^{pos}$ or $CD14^{neg}$ were plated out on matrigel in triplicates. After 7-12 days colonies were counted and passaged as a single cell suspension again (N= 4 mice). 4 independent experiments were performed and the average is shown, P=0.7, 0.9 (NS: non-significant). Values represent mean ± s.d. Student's unpaired t-test for independent samples was used.

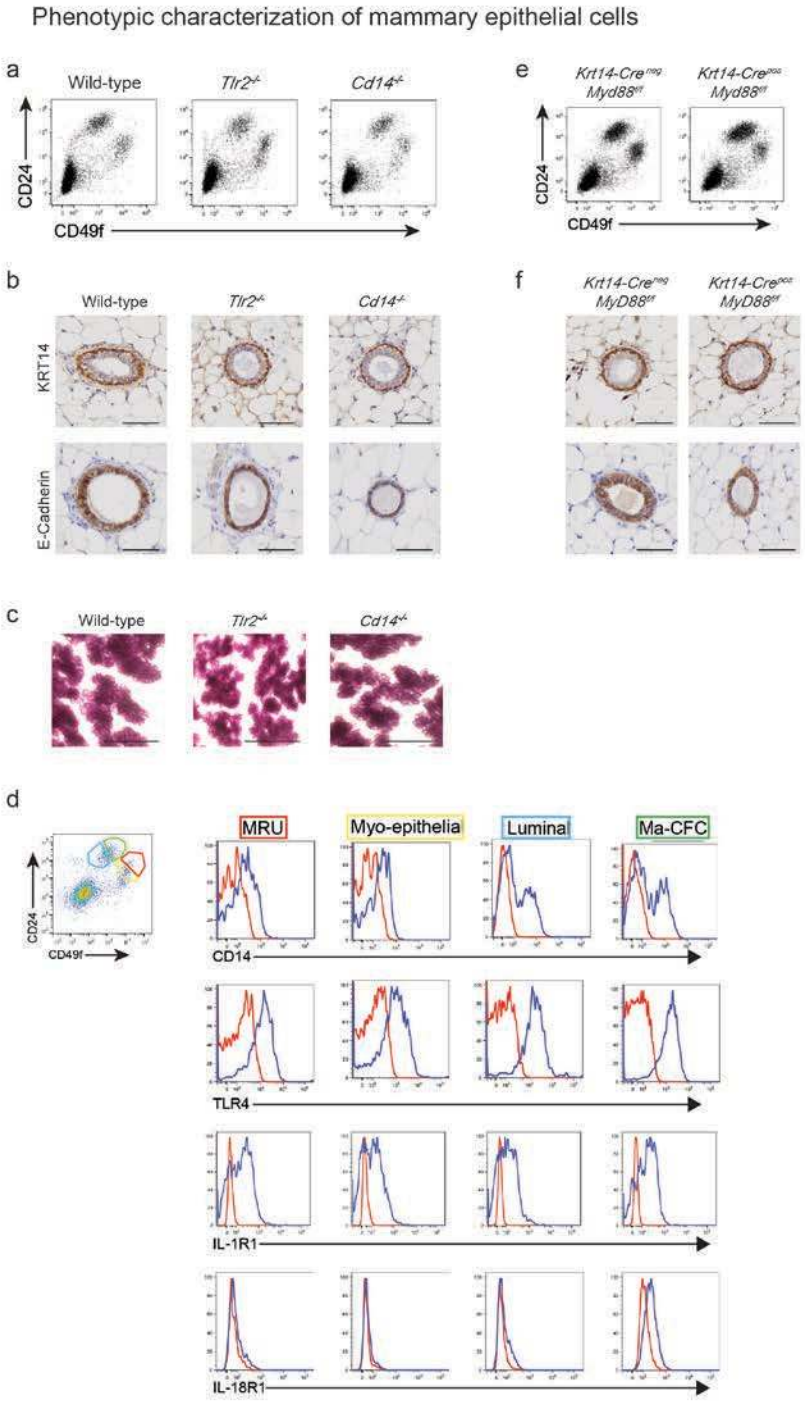

Supplementary Figure 2 Phenotypic characterization of mammary epithelial cells. **(a)** Flow cytometric analysis of mammary epithelial cells from 6 weeks old mice of wild-type, *Tlr2*$^{-/-}$ and *Cd14*$^{-/-}$ mice. Cells were gated on life and lineage negative cells. (**b**) Immunohistochemistry on mammary glands from 6 weeks old mice of wild-type, *Tlr2*$^{-/-}$ and *Cd14*$^{-/-}$ mice. Myoepithelial cells (Cytokertain-14 (KRT14)) and luminal cells (E-CADHERIN) are present and properly organized in both wild-type as well as the knock out mammary glands. Scale bar is 50 µm (c) Carmine Alum staining on whole mount of lactation of wild-type, *Tlr2*$^{-/-}$ and *Cd14*$^{-/-}$ mice. Scale bar is 1 mm. (**d)** Flow cytomety analysis of mammary epithelial cells from 6-8 weeks old mice. Cells were gated on live and lineage negative and stained for CD24, CD49f and CD14, TLR4, IL-1R1 or IL-18R1. In red is the isotype control for each specific sub-population, in blue is the CD14, TLR4, IL-1R1 or IL-18R1 staining. (**e**) Flow cytometry analysis of *Myd88*$^{-/-}$ mammary epithelial cells, from 6 weeks old mice of *Krt14-Cre*^{neg}*Myd88*$^{f/f}$ and *Krt14-Cre*^{pos}*Myd88*$^{f/f}$ mice. Cells were gated on life and lineage negative cells. (**f**) Immunohistochemistry on mammary glands from 6 weeks old mice of *Krt14-Cre*^{neg}*Myd88*$^{f/f}$ and *Krt14-Cre*^{pos}*Myd88*$^{f/f}$ mice. Myoepithelial cells (Cytokertain-14 (KRT14)) and luminal cells (E-CADHERIN) are present and properly organized in the *MyD88* knockout mammary gland. Scale bar is 50 µm. All analyses were done with at least 3 mice.

Limiting dilutions o f mammmary epithelial cells.

a

# of Lin Neg cells	WT	*Tlr2* KO	*Cd14* KO
25K	15/20	4/9	1/6
10K	15/18	1/10	0/10
5K	9/14	3/20	3/10
2.5K	6/11	2/20	2/12
1.25K	0/12	0/16	0/8

b

# of cells	WT	*Tlr4* KO
10K	5/8	4/10
5K	4/6	3/10
2.5K	6/11	1/10

c

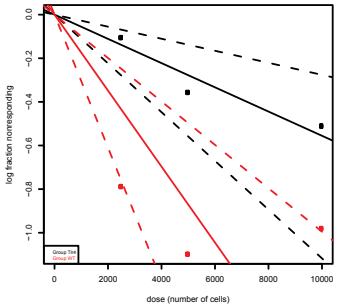

Genotype	MRU frequency	±SE	p-Value
WT	1/5741	3280-10049	
Tlr4 KO	1/18005	8948-36227	0.0085

d

# of cells	WT	*Il-1r1* KO	*Il-18r1* KO
25K	15/20	12/12	5/6
10K	15/18	11/16	3/8
5K	9/14	10/16	5/9
2.5K	6/11	11/16	3/9
1.25K	0/12	3/14	0/7

e

# of Lin Neg cells	WT	*Tlr2* KO	*Ink4A-Arf* KO	*Tlr2* KO *Ink4A-Arf* KO
25K	3/4	4/9	7/7	6/6
10K	5/8	1/10	12/20	5/10
5K	4/6	3/20	9/19	4/13
2.5K	6/11	2/20	3/14	2/12
1.25K	0/12	0/16	2/6	1/4

f

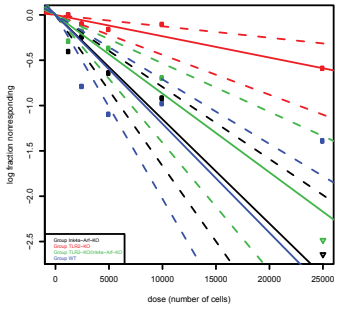

Genotype	MRU frequency	±SE	p-Value
WT	1/8322	4928-14055	
Tlr2 KO	1/42476	22714-79433	<0.0001
Ink4a-Arf KO	1/8691	6004-12580	N.S.
Tlr2 KO *Ink4a-Arf* KO	1/11515	7091-18698	N.S.

Supplementary Figure 3 Limiting dilutions of mammary epithelial cells. In order to determine the MRU frequency of each donor genotype we injected sorted cells, as indicated from donor mice of 10 to 14 weeks old mice in cleared mammary fat pads of three weeks old recipients. Recipient mice were syngeneic C57BL/6J mice. Numbers of successful out growths and numbers of total injections are shown for each dilution and genotype. MRU frequency and confidence was determined by ELDA graph and analysis. a) Raw numbers for limiting dilutions of *Tlr2*$^{-/-}$ and *Cd14*$^{-/-}$ lin^{neg} MECs for figure 4a. b-c) Raw numbers for limiting dilutions of *Tlr4*$^{-/-}$ lin^{neg} MECs, including ELDA analysis. Data for WT (N=25 samples), *Tlr4*$^{-/-}$ (N=30 samples) pooled from 3 independent experiments. P=0.0085. d) Raw numbers for limiting dilutions of *Il-1r1*$^{-/-}$ (N=74 samples) and *Il-18r1*$^{-/-}$ lin^{neg} (N=39 samples) MECs. e-f) Limiting dilutions of *Ink4a-Arf*$^{+/+}$ *Tlr2*$^{+/+}$(WT), *Ink4a-Arf*$^{+/+}$ *Tlr2*$^{-/-}$ (*Tlr2* KO), *Ink4a-Arf*$^{-/-}$ *Tlr2*$^{+/+}$ (*Ink4a-Arf* KO) and Ink4a-Arf$^{-/-}$ Tlr2$^{-/-}$ (*Ink4a-Arf* KO *Tlr2* KO) lin^{neg} MECs, including ELDA graph and analysis. Data for WT (N=41 samples), *Tlr2*$^{-/-}$ KO (N=75 samples), P<0.0001, *Ink4a-Arf* KO (N=66 samples), P=N.S. and *Ink4a-Arf* KO *Tlr2* KO (N=45 samples), P=N.S. are pooled from 4 independent experiments.

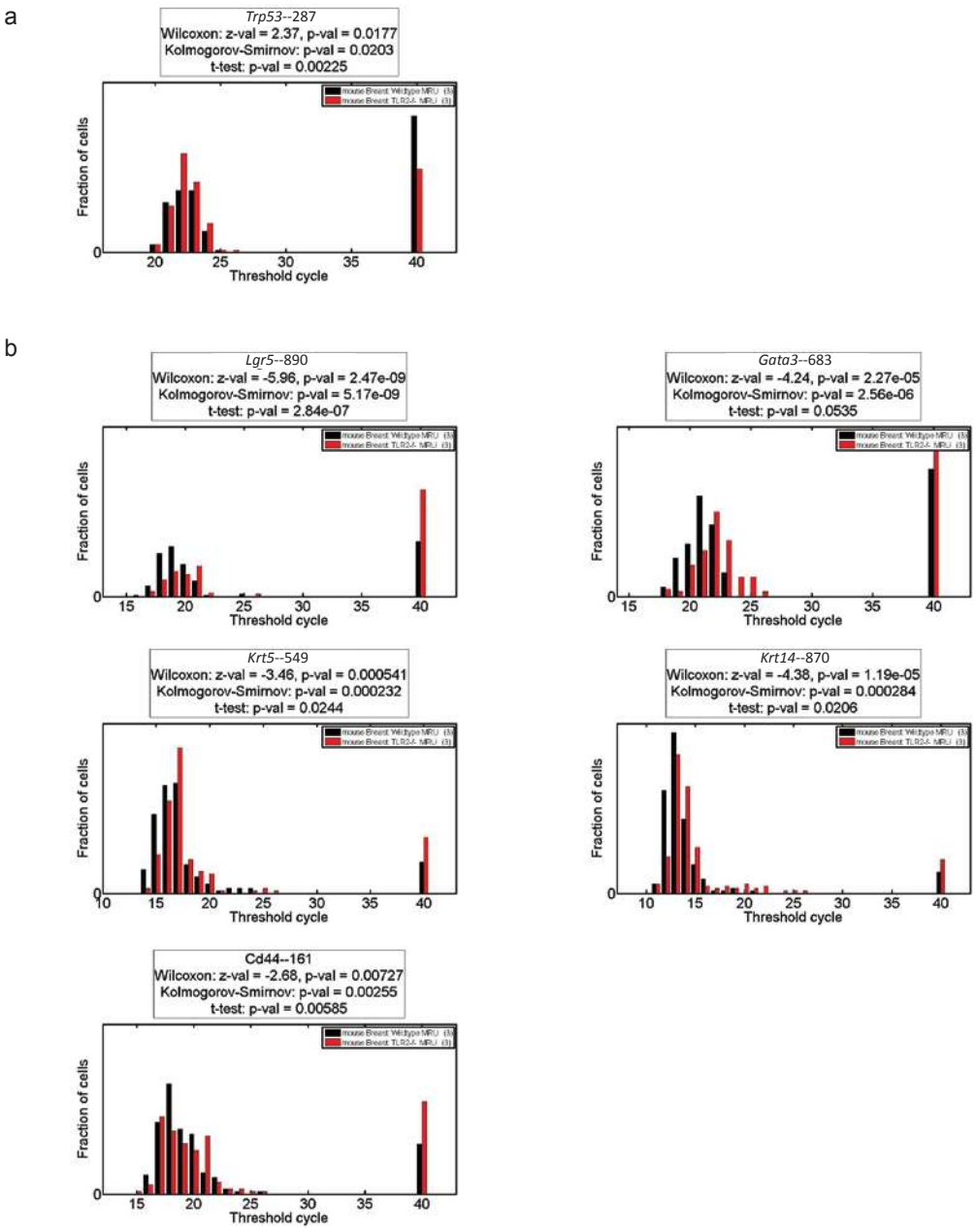

Supplementary Figure 4 Single cell gene expression of MRU. Single cell expression showing expression of wild-type (black) and *Tlr2*$^{-/-}$ (red) MRUs for figure 3e. Cells were double sorted and subjected to multiplexed single cell rt-PCR. Normalized Ct values as visualized by comparing the distribution of Ct values in histograms. (**a**) Gene that was significantly up-regulated in *Tlr2*$^{-/-}$ cells as compared to wild-type cells. (**b**) Genes that were significantly down-regulated in *Tlr2*$^{-/-}$ as compared to wild-type cells. Each analysis was done on 2 different mice.

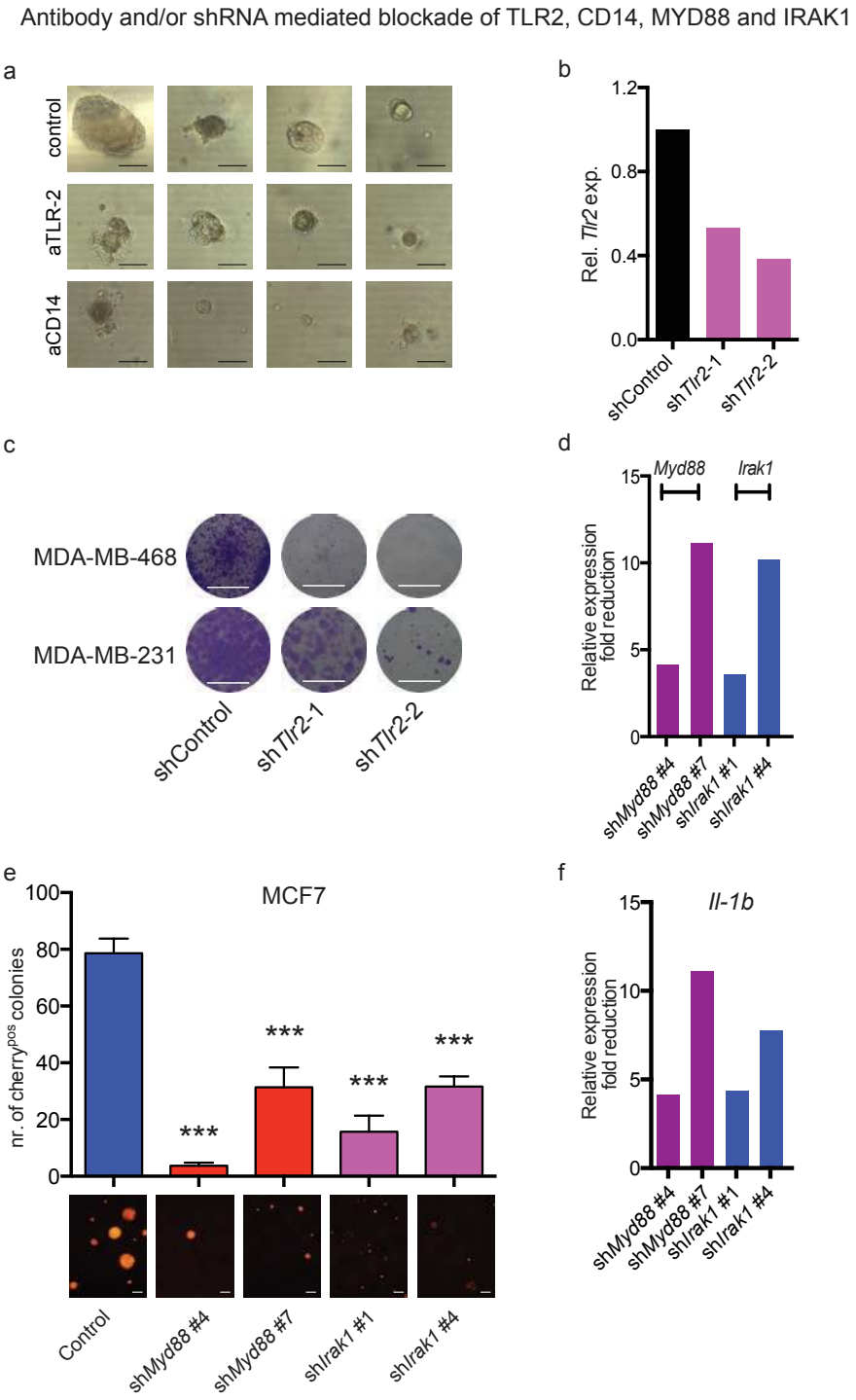

Supplementary Figure 5 Antibody and/or shRNA mediated blockade of TLR2, CD14, MYD88 and IRAK1. (**a**) Representative examples colony formation on matrigel of primary ER^{neg} breast cancer cells (N=4). Scale bar is 20 µm. Cells were treated with control antibody or with neutralizing TLR2 and CD14 antibodies. (**b-c**) Two breast cell lines were transduced with the lentivirus to knockdown TLR2 and after puromycin selection cells were plated out and stained with crystal violet blue after 9 days in culture. Data are representative of 2 experiments. Scale bar is 1 cm. (**d**) MDA-MD-231 cells were transduced with control or indicated shRNA and knock-down efficiency was determined by qPCR. All shRNA mediated knock-down constructs resulted in a 4 to 12x reduction of its target mRNA. Data are representative of 2 experiments. (**e**) Knock-down of MYD88 and IRAK1 in the breast cell line MCF7. After transduction cells were sorted for Cherry and plated out on matrigel in triplicate to determine colony forming capacity. The number of colonies on matrigel is shown and a representative photo of the colonies is shown. N=6 samples pooled from 2 independent experiments. ***, $p<0.001$. Scale bar is 20 µm. Values represent mean ± s.d. Student's unpaired t-test for independent samples was used. (**f**) MYD88 and IRAK1 knock down resulted in decreased expression of the NF-KB target gene IL-1B indicating that the knock down resulted in decreased NF-KB activity. Data are representative of 2 experiments.

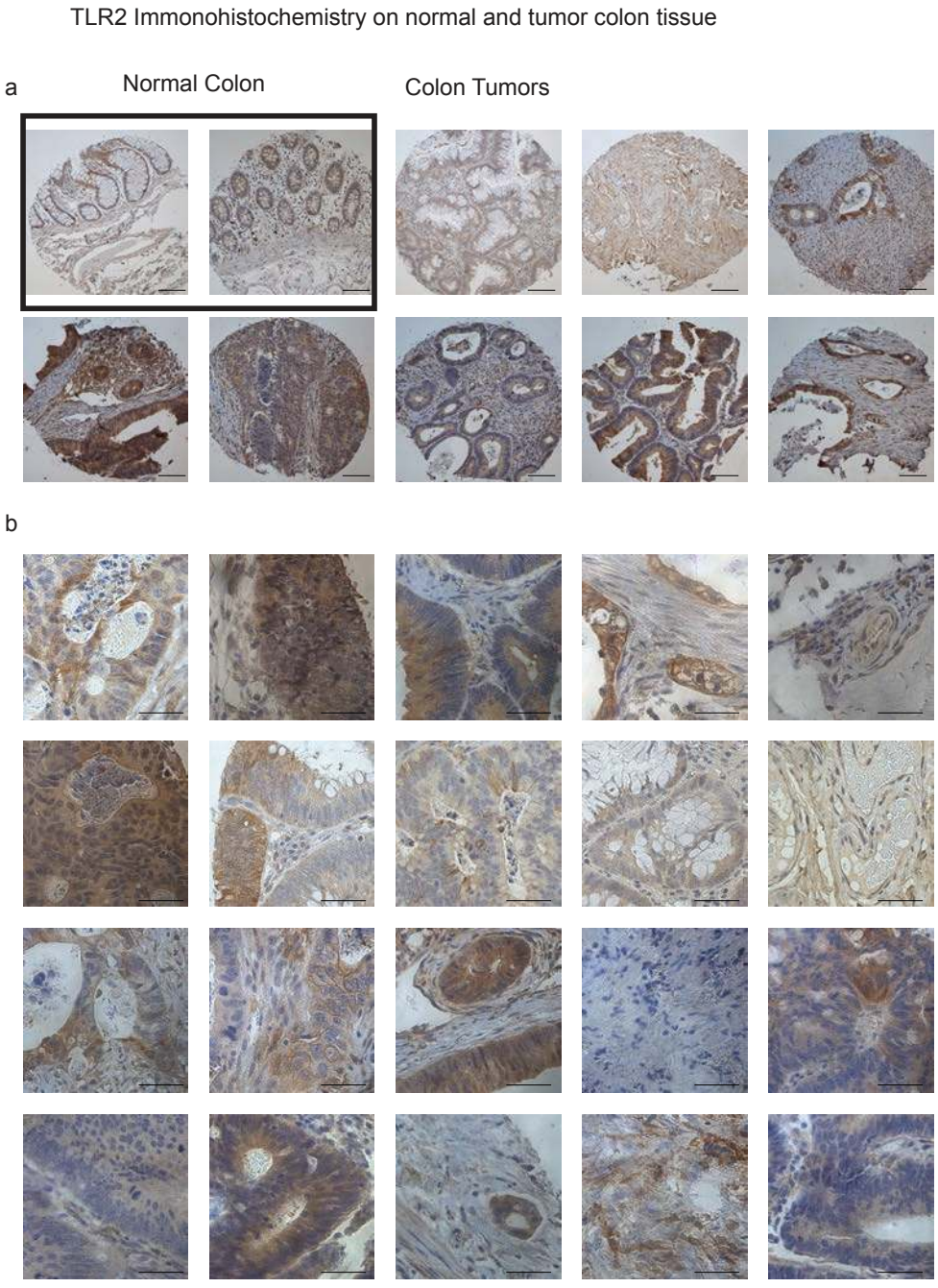

Supplementary Figure 6 TLR2 immunohistochemistry on normal and tumor colon tissue. (**a**) 10X magnification of immunohistochemistry for TLR2. Boxed is normal colon tissue, the rest are colon tumors. Scale bar is 200 μm (**b**) 40X magnification of immunohistochemistry for TLR2 of colon tumors. Scale bar is 50 μm.

Genome editing the *Tlr2* locus using CAS9

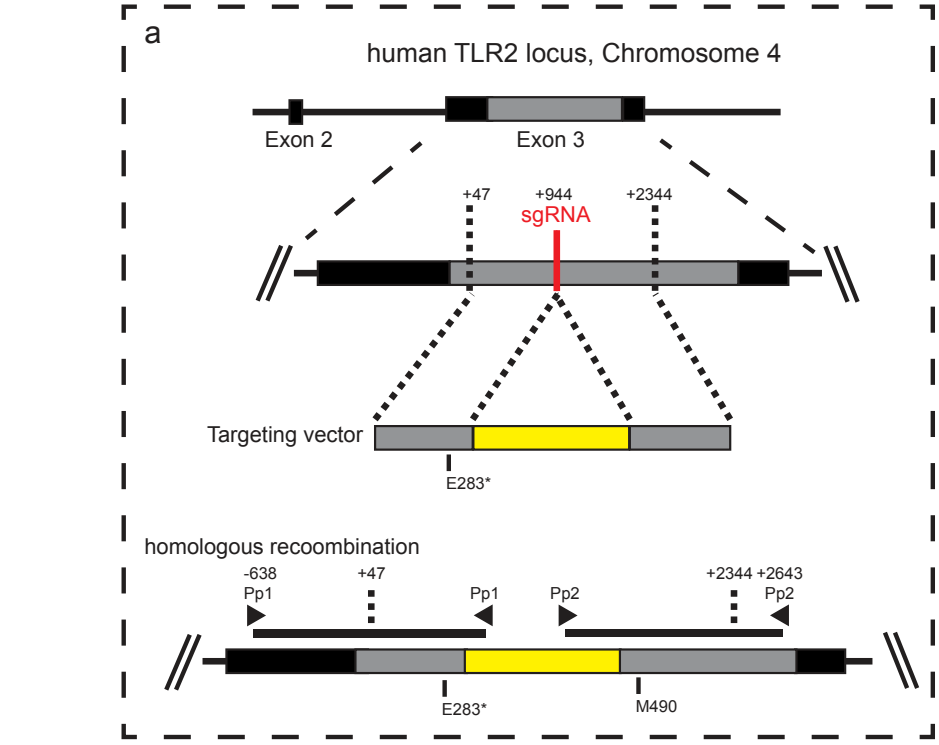

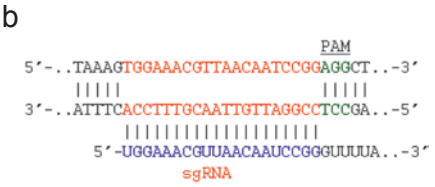

c

Genomic junction of HR with genomic DNA

Primer set 1 junctions:

TLR2 outside HR TLR2 HR

...TTTTGGGTAAATCTGAGAGCTGCGATAAAGTCCTAGGTTCCCATATTTAA.....

TLR2 HR CMV-Cherry-pA

.....TGGAATATGCAGCCTCCGGATTGTTCGCGTTAAGATACATTGATGAGTTT...

Primer set 2 junctions:

CMV-Cherry-pA TLR2 HR

...AAACTCATCAATGTATCTTAACGCGAACAATCCGGAGGCTGCATATTC.....

TLR2 HR TLR2 outside HR construct

.....TTTGGGTAAATCTGAGAGCTGCGATAAAGTCCTAGGTTCCCATATTTAA...

Supplementary Figure 7 Genome editing the *Tlr2* locus using CAS9. (**a**) Schematic of the targeted region of human TLR2 locus and targeting strategy. sgRNA cuts around +944. The homologues recombination (HR) cassette has a left arm (including the E283* mutation) and a right arm. In between there is a CMV Cherry pA cassette (yellow box) in the anti sense orientation. Primer pairs (Pp1 & Pp2) are shown to detect homologues recombination. (**b**) Region of the sgRNA complementary to the protospacer. c) Sequenced region show correct integration of HR construct as determined by sequencing the genomic junctions.